

Human connexin26 and connexin30 form functional heteromeric and heterotypic channels

Sabrina W. Yum, Junxian Zhang, Virginijus Valiunas, Giedrius Kanaporis, Peter R. Brink, Thomas W. White and Steven S. Scherer

Am J Physiol Cell Physiol 293:1032-1048, 2007. First published Jul 5, 2007;
doi:10.1152/ajpcell.00011.2007

You might find this additional information useful...

Supplemental material for this article can be found at:

<http://ajpcell.physiology.org/cgi/content/full/00011.2007/DC1>

This article cites 69 articles, 28 of which you can access free at:

<http://ajpcell.physiology.org/cgi/content/full/293/3/C1032#BIBL>

Updated information and services including high-resolution figures, can be found at:

<http://ajpcell.physiology.org/cgi/content/full/293/3/C1032>

Additional material and information about *AJP - Cell Physiology* can be found at:

<http://www.the-aps.org/publications/ajpcell>

This information is current as of September 12, 2007 .

Human connexin26 and connexin30 form functional heteromeric and heterotypic channels

Sabrina W. Yum,¹ Junxian Zhang,² Virginijus Valiunas,³ Giedrius Kanaporis,³ Peter R. Brink,³ Thomas W. White,³ and Steven S. Scherer²

¹Section of Neurology, St. Christopher's Hospital for Children, Drexel University College of Medicine, Philadelphia, Pennsylvania; ²Department of Neurology, University of Pennsylvania, Philadelphia, Pennsylvania; and ³Department of Physiology and Biophysics, State University of New York, Stony Brook, New York

Submitted 9 January 2007; accepted in final form 29 June 2007

Yum SW, Zhang J, Valiunas V, Kanaporis G, Brink PR, White TW, Scherer SS. Human connexin26 and connexin30 form functional heteromeric and heterotypic channels. *Am J Physiol Cell Physiol* 293: C1032–C1048, 2007. First published July 5, 2007; doi:10.1152/ajpcell.00011.2007.—Mutations in *GJB2* and *GJB6*, the genes that encode the human gap junction proteins connexin26 (Cx26) and connexin30 (Cx30), respectively, cause hearing loss. Cx26 and Cx30 are both expressed in the cochlea, leading to the potential formation of heteromeric hemichannels and heterotypic gap junction channels. To investigate their interactions, we expressed human Cx26 and Cx30 individually or together in HeLa cells. When they were expressed together, Cx26 and Cx30 appeared to interact directly (by their colocalization in gap junction plaques, by coimmunoprecipitation, and by fluorescence resonance energy transfer). Scrape-loading cells that express either Cx26 or Cx30 demonstrated that Cx26 homotypic channels robustly transferred both cationic and anionic tracers, whereas Cx30 homotypic channels transferred cationic but not anionic tracers. Cells expressing both Cx26 and Cx30 also transferred both cationic and anionic tracers by scrape loading, and the rate of calcein (an anionic tracer) transfer was intermediate between their homotypic counterparts by fluorescence recovery after photobleaching. Fluorescence recovery after photobleaching also showed that Cx26 and Cx30 form functional heterotypic channels, allowing the transfer of calcein, which did not pass the homotypic Cx30 channels. Electrophysiological recordings of cell pairs expressing different combinations of Cx26 and/or Cx30 demonstrated unique gating properties of cell pairs expressing both Cx26 and Cx30. These results indicate that Cx26 and Cx30 form functional heteromeric and heterotypic channels, whose biophysical properties and permeabilities are different from their homotypic counterparts.

gap junctions; hearing; fluorescence resonance energy transfer; fluorescence recovery after photobleaching; immunoprecipitation; dye transfer; electrophysiology

GAP JUNCTIONS ALLOW THE INTERCELLULAR passage of ions and small molecules up to ~5,000 Da (59) and are thought to have diverse functions, including the propagation of electrical signals, metabolic cooperation, spatial buffering of ions, growth control, and cellular differentiation (8). They are formed by two apposed hemichannels (or connexons); a complete channel is formed when one hemichannel docks with a compatible hemichannel on an apposed cell membrane. Each hemichannel is comprised of six compatible connexin molecules, a large family of highly conserved proteins, usually named according to their predicted molecular mass (64). Individual hemichan-

nels can be composed of one (homomeric) or more than one (heteromeric) type of connexin. Similarly, channels can be composed of hemichannels containing the same (homotypic) or different (heterotypic) connexins (34, 63). Any two compatible connexins can theoretically form 196 different channels (7).

Mutations in *GJB2* and *GJB6*, the genes that encode the human gap junction proteins connexin26 (Cx26) and connexin30 (Cx30), cause hearing loss (43). The Connexin-Deafness homepage is <http://davinci.crg.es/deafness>. Recessive mutations of *GJB2/Cx26* are the most common cause of nonsyndromic hearing loss, accounting for 50% of such patients. Dominant mutations in *GJB2/Cx26* (either in isolation or as part of a syndrome that includes a variety of skin diseases) and *GJB6/Cx30* also cause hearing loss. Cx26 and Cx30 are coexpressed in the affected tissues, the cochlea, and the skin (2, 22, 33, 35, 44), so that altered functions of these proteins in the cells that express them likely account for the disease manifestations (cell autonomous effects).

Cx26 and Cx30 have broadly overlapping (but not identical) distributions and a similar profile of developmental expression (2, 23, 28, 49, 71) in rodent cochlea. It has been suggested that hybrid Cx26 and Cx30 channels may be required for normal hearing, as ablation of Cx30 or Cx26 result in hearing loss, despite continuing expression of Cx26 or Cx30 (13, 50). Cx26 and Cx30 have been coimmunoprecipitated from mouse cochlear homogenates (2, 22, 49) and from transfected cells that coexpress mouse (49) or human (16) Cx26-enhanced green fluorescent protein (EGFP) and Cx30-EGFP. Whether human Cx26 and Cx30 without epitope tags can form hybrid channels has not been demonstrated, which is a potentially important question, as species specificity of channel properties have been reported and epitope-tagged connexins may potentially affect the biophysical properties of the channels (4, 5, 9, 25, 48). To investigate this issue, we expressed human Cx26 and Cx30 individually or together in HeLa cells. Our results indicate that human Cx26 and Cx30 form functional heteromeric and heterotypic channels, whose biophysical properties and permeabilities are different from their homotypic counterparts.

MATERIALS AND METHODS

Generating Cx26 and Cx30 expression constructs. A plasmid containing human *GJB2/Cx26* (kindly provided by Dr. Bruce Nicholson) was amplified by PCR using oligonucleotide primers designed to include the open reading frame and incorporate a 5' *NheI* site and a

Address for reprint requests and other correspondence: S. W. Yum, Section of Neurology, St. Christopher's Hospital for Children, Erie Ave. at Front St., Philadelphia, PA 19134 (e-mail: ssy25@drexel.edu).

The costs of publication of this article were defrayed in part by the payment of page charges. The article must therefore be hereby marked "advertisement" in accordance with 18 U.S.C. Section 1734 solely to indicate this fact.

3' *Bam*HI site, using Platinum *Pfx* DNA polymerase (Invitrogen, Carlsbad, CA). Cx30 was obtained by RT-PCR (Superscript II; Invitrogen) from human corpus callosum RNA (Clontech, Palo Alto, CA), using oligonucleotide primers (sense: 5'-GTACGATATCACAGGACT-CAGGGATAAACCC, antisense: 5'-CAGAGGATCCCAGAAGTCTC-CTTATGACGC) designed to amplify the open reading frame and incorporate a 5' *Eco*RV site and a 3' *Bam*HI site, using Proofstart polymerase (Qiagen, Valencia, CA). Cx26 and Cx30 PCR products were digested with *Nhe*I and *Bam*HI or *Eco*RV and *Bam*HI, respectively, ligated into pIRESneo3 and/or pIRESpuo3 (Clontech), and the resulting constructs were used to transform DH5 α -competent cells. A large-scale plasmid preparation was made from a single colony (Qiagen) and sequenced at the Cell Center at the University of Pennsylvania. The correct sequences were confirmed by comparison with published *GJB2/Cx26* (GenBank NM004004.3) or *GJB6/Cx30* sequences. Sequence of our Cx30 clone (GenBank accession no. AY297110) showed two nucleotide differences from the published sequence (GenBank accession nos. NM006783 and AJ005585). The first change (A to C at base 108) did not alter the deduced amino acid sequence, and the second change (C to G at base 372) was predicted to result in H124Q amino acid change. We found a perfect match of our cDNA sequence with the sequence of the Human Genome Project (NT_024524.13 and NT_086801.1), the NEDO human cDNA sequencing project (GenBank accession no. AK075242), and the sequence of another human clone (BC038934). To generate connexin-ECFP or connexin-enhanced yellow fluorescent protein (EYFP) constructs, cDNAs of human Cx26, Cx30, or Cx43 were amplified by PCR using oligonucleotide primers designed to include the open reading frame, delete the stop codon, and incorporate a 5' *Eco*RI site and a 3' *Bam*HI site, using *Pfu* Turbo polymerase. The PCR products were cloned into the *Eco*RI and the *Bam*HI restriction sites of vector pECFPN1 or pEYFPN1 (Clontech). The resulting constructs included the cDNA sequences of the autofluorescent reporter proteins ECFP or cyan-yellow fluorescent protein (CYFP) fused in-frame to the COOH terminus of the open reading frame of specific connexin with a seven-amino acid linker. A large-scale plasmid preparation was made from a single colony, and all constructs were verified by automated DNA sequence as described above.

Generating cell lines expressing Cx26, Cx30, or Cx30 and Cx26. Communication-incompetent HeLa cells (19) were grown in six-well plates, and transfection was carried out using Lipofectamine 2000 (Invitrogen) as described (66). Two days after transfection, HeLa cells were selected by adding 1 μ g/ml puromycin (Sigma-Aldrich, St. Louis, MO) to the medium over 3 wk. The cells were trypsinized and plated at low density, and single colonies were picked and expanded. Cloned cells stably expressing Cx26 or Cx30 were obtained by screening at least 30 different clones by immunostaining; of these, ~8 showed stable expressions for at least 8 wk.

To generate cells expressing both Cx30 and Cx26, we transfected one cloned cell line that stably expressed Cx30 with Cx26 in pIRESneo3 (or empty vector pIRESneo3) according to the protocol described above. After selection with both 1 μ g/ml of puromycin and 1 mg/ml of G418 (Invitrogen) for ~3 wk, the colonies were trypsinized, and these bulk-selected cells were expanded for further studies.

Immunocytochemistry. HeLa cells were grown on coverslips for 2 days, and immunocytochemistry was performed as described (66). We screened for antibodies against Cx26 that did not cross-react with Cx30 and antibodies against Cx30 that did not cross-react with Cx26 by immunostaining cells that stably expressed Cx26 or Cx30. In this way, we found a monoclonal antibody (Zymed Laboratories 33-5800, South San Francisco, CA; diluted 1:500) and a rabbit antiserum (Zymed Laboratories 51-2800, diluted 1:1,000), both against the COOH terminus of Cx26, and a rabbit antiserum against the COOH terminus of Cx30 (Zymed Laboratories 71-2200, diluted 1:1,000) that did not cross-react. We used these antibodies in our experiments,

typically the combination of the mouse anti-Cx26 and the rabbit anti-Cx30.

Immunoblot analysis and coimmunoprecipitations. HeLa cells were harvested, the pellets were lysed, and the protein lysates were separated by SDS-PAGE, transferred over 1 h as described (66). To screen for antibodies against Cx26 that did not cross-react with Cx30 and antibodies against Cx30 that did not cross-react with Cx26, the blots were incubated with various primary antibodies against either Cx30 or Cx26 overnight at 4°C. Subsequently, the blots were incubated in peroxidase-coupled donkey antiserum against rabbit or mouse IgG (Jackson ImmunoResearch, West Grove, PA; diluted 1:10,000) for 1 h at room temperature and visualized by enhanced chemiluminescence (Amersham, Piscataway, NJ). In this way, we found that the antibodies that did not cross-react by immunostaining (described above) also did not cross-react by immunoblotting (Fig. 2). These antibodies were used in the coimmunoprecipitation analysis.

For coimmunoprecipitations, HeLa cells grown to confluence on 60-mm plates were lysed in 500 μ l of ice-cold RIPA buffer (10 mM sodium phosphate, pH 7.0, 150 mM NaCl, 2 mM EDTA, 50 mM sodium fluoride, 1% Nonidet P-40, 1% sodium deoxycholate, and 0.1% SDS) for 15 min on ice, scraped, and then spun at 14,000 rpm for 30 min. The supernatants were collected and incubated on ice with either 10 μ l of mouse monoclonal antibody against Cx26 (Zymed Laboratories 33-5800) or 5 μ l of rabbit antiserum against Cx30 (Zymed Laboratories 71-2200) for 1 h. Protein G agarose (100 μ l) was added to the above cell lysate/antibody solution and incubated overnight at 4°C. The beads were washed in RIPA buffer, resuspended in electrophoresis buffer (62.5 mM Tris, 20% glycerol, 2% SDS, 100 mM DTT), and separated on a 12% SDS-polyacrylamide gel for protein detection following the immunoblotting protocol described. The blots were initially incubated with rabbit polyclonal antiserum against either Cx30 (Zymed Laboratories 71-2200, diluted 1:10,000) or Cx26 (Zymed Laboratories 51-2800, diluted 1:1000), visualized, and then rehybridized with a rabbit antiserum against Cx26 or Cx30, respectively. For negative control, Cx26 stable cells transiently transfected with human Cx43 were immunoprecipitated with mouse monoclonal antibody against Cx26, blotted with rabbit polyclonal antiserum against Cx43 (Zymed Laboratories, diluted 1:10,000), and rehybridized with the rabbit antiserum against Cx26.

Fluorescence resonance energy transfer assay. For fluorescence resonance energy transfer (FRET), HeLa cells were fixed with 4% paraformaldehyde 24 h after cotransfection with equal amounts of plasmids encoding Cx-ECFP (donor) and Cx-EYFP (acceptor). To minimize the bleeding through of the ECFP emission into the EYFP emission, and vice versa, as is frequently encountered in acceptor-depletion FRET, we adopted the method of acceptor-depletion FRET with linear spectral unmixing (u-ad FRET) described by Gu and colleagues (16, 26). We acquired λ stacks, each consisting of images from eight contiguous but nonoverlapping spectral channels (each 11 nm in bandwidth), extending from near the peak of the ECFP emission (474 nm) to near the peak of the EYFP emission (562 nm) with a Fluoview FV1000 Olympus laser scanning confocal microscope ($\times 60$, oil immersion objective). Two argon laser lines were used: the 458-nm line of a 30-mW laser at 0.3% excitation power was used for simultaneous imaging of both ECFP and EYFP, and the 514-nm laser line was used for acceptor photobleaching because it excites only EYFP. Three λ stacks were obtained, and preselected regions of interest (ROIs) were repeatedly photobleached (with the 514-nm laser) 15–20 times at 100% excitation power so that the EYFP signal was eliminated within the ROIs. After photobleaching, three more λ stacks were obtained. Each individual λ stack was subjected to linear unmixing using reference spectra from images of cells transfected with Cx26-ECFP, Cx30-ECFP, Cx26-EYFP, or Cx30-EYFP. The mean pixel density of ECFP and EYFP within ROIs from these “unmixed images” was exported (as an Excel file) for further analysis using the interactive software of the Olympus microscope (see sup-

plemental Fig. S2). (Supplemental materials for this article are available online at the *Am J Physiol Cell Physiol* website.)

For each ROI, the mean pixel density of the three unmixing images was averaged, for both the donor (ECFP) and the acceptor (EYFP), before (ECFPpre and EYFPpre) and after (ECFPpost and EYFPpost) photobleaching. These data were used to calculate the FRET efficiency, the relative donor (D) and acceptor (A) concentration ratio (D-A ratio), and the acceptor emission (A-level) as previously described (26, 31, 67): FRET efficiency (%) = $100 \times (\text{ECFPpost} - \text{ECFPpre}) / \text{ECFPpost}$; D (%) = $100 \times \text{ECFPpost} / (\text{ECFPpost} + \text{EYFPpre})$; A (%) = $100 \times \text{EYFPpre} / (\text{ECFPpost} + \text{EYFPpre})$; D-A ratio = D/A; and A-level = EYFPpre.

The FRET efficiency was measured only in regions where the D-A ratio was within 0.33 and 3 to avoid calculation errors caused by low signal-to-noise ratio and FRET efficiency saturation (16, 30). The data were processed, and statistical analysis was performed with the GraphPad Prism 4 software (GraphPad Software, San Diego, CA).

Scrape loading and fluorescence recovery after photobleaching. For scrape loading, HeLa cells were grown to confluence on 60-mm plates, and the medium was changed to HBSS (without Ca^{2+} or Mg^{2+}) plus one of the following fluorescence dyes: 0.1% Lucifer yellow (LY), 1 mM 5,6-carboxyfluorescein (CF), 0.1% ethidium bromide (EB), or 0.3% propidium iodide (PI), all from Sigma-Aldrich, as well as 2% neurobiotin (NB), a nonfluorescent tracer (Vector Laboratories, Burlingame, CA). A scalpel blade was used to make many parallel lines on the dish; after 5 min, cells were washed with HBSS and imaged with both fluorescence and phase-contrast optics. Cells scrape loaded with NB were fixed for 10 min in 4% paraformaldehyde, blocked (5% fish skin gelatin in PBS containing 0.1% Triton), and incubated with streptavidin-rhodamine (1:300) for 1 h at room temperature. After washing, coverslips were mounted with Vectashield and samples were photographed under a Leica fluorescence microscope with Hamamatsu digital camera C4742-95 connected to a G5 Mac computer, using the Openlab 2.2 software. Scrape loading was quantified by measuring the distance from the scrape line to the point where the fluorescence intensity dropped to $1.5 \times$ the background intensity. For each cell line, this was measured for EB, PI, and NB by acquiring at least eight images from each of three different plates of cells. The images were processed and analyzed with NIH ImageJ software, and the mean distance was calculated with Microsoft Excel software and compared between cell lines using ANOVA (GraphPad Prism 4 software, San Diego, CA).

For fluorescence recovery after photobleaching (FRAP), cells were grown on a 35/22-mm glass bottom dish (Warner Instruments, Hamden, CT) for ~40 h to 70–90% confluence, washed in HBSS, and incubated with calcein-AM (1 μM ; Biotium, Haywood, CA) in Opti-MEM (Invitrogen) for 20 min, rinsed several times with HBSS, and maintained in Opti-MEM at room temperature during the experiment. With a $\times 60$ objective and the interactive software of a Fluoview FV1000 Olympus laser scanning confocal microscope, we used the 488-nm line of a 30-mW Argon laser at 0.3% excitation power to detect the green fluorescence signal during the entire recording. Individual cells that were surrounded by at least four other cells were photobleached for 600 ms with a 405-nm, 25-mW diode laser at full power. The aim was to bleach maximally the selected cells, without bleaching neighboring cells.

To measure FRAP, images were acquired before bleaching and every 10 s after bleaching for 500 s, and average fluorescence intensity in the bleached cell in every image was measured as mean pixel density and exported as Excel files. One unbleached cell in the same field was also monitored for fluorescence loss throughout the experiment. In addition, individual cells that were isolated from the rest of the cells were also bleached and monitored for recovery in each dish; no recovery was observed (data not shown). Using Microsoft Excel software, the fluorescence signal intensity immediately before and immediately after photobleaching was normalized to 100% and 0%, respectively. Recovery was calculated based on the fluores-

cence intensity in the photobleached cell at each time point relative to the fluorescence intensity of the same cell at the same region before the bleaching and expressed as percent recovery.

For analysis of heterotypic gap junction dye coupling, one cell type was pre-labeled with cell membrane dye DiI (10 $\mu\text{g}/\text{ml}$, Molecular Probes) for 20 min at 37°C. The cells were trypsinized and mixed with unlabeled cells at a ratio of 1:30, and FRAP was performed after 24–30 h as described above. The 543-nm argon laser line was used to detect the DiI fluorescence signal. To minimize phototoxicity to the cells, this image laser was turned off after the prebleaching image was obtained. Individual cells labeled with DiI (surrounded by at least 4 unlabeled cells) were selected for photobleaching. Because DiI served as a marker to identify the heterotypic cell pairs, it was never bleached during the experiment. To verify the fidelity of DiI prelabeling, one plate of cells was labeled with DiI and another plate of cells was labeled with DiO (10 $\mu\text{g}/\text{ml}$; Molecular Probes), which is a similar lipophilic dye with a different fluorescence. After coculture for 24–30 h, all cells were either DiI or DiO positive; there were no unlabeled cells and no cells were double labeled (data not shown).

Statistical analyses of the FRAP results were conducted to determine whether the slope of the curves differed from each other. A regression model with autocorrelated errors was applied to model recovery curve over time using the SAS software version 9.1, and the three parameters in the model (coefficients of quadratic term and linear term of time, as well as the constant term in the formula) between two cell lines were compared. A *P* value of <0.05 was considered to be significant.

Electrophysiological studies. Electrical measurements were performed 1–3 days after cell plating. Glass coverslips with adherent cells were transferred to an experimental chamber mounted on the stage of an inverted microscope (Olympus IMT2) and superfused at room temperature (21–23°C) with bath solution containing (in mM) 140 NaCl, 5 KCl, 2 CaCl_2 , 1 MgCl_2 , 5 glucose, and 5 HEPES (pH 7.4). The patch pipettes were pulled from glass capillaries (GC150F-10; Harvard Apparatus, Edenbridge, UK) with a horizontal puller (DMZ-Universal; Zeitz-Instrumente, Augsburg, Germany) and were filled with saline containing (in mM) 120 potassium aspartate, 10 NaCl, 3 MgATP, 10 EGTA (pCa ~8), and 5 HEPES (pH 7.2). When filled, the resistance of the pipettes measured 1–3 M Ω . Experiments were carried out on cell pairs using a double-voltage patch-clamp technique, which allowed us to control the membrane potential and transjunctional voltage (V_j) of both cells and to measure associated junctional currents (56). In experiments carried out on mixed cell pairs, the Cell Tracker green (Molecular Probes) was used to allow heterologous pairs to be identified (60).

Signal recording and analysis. Voltage and current signals were recorded with patch-clamp amplifiers (Axopatch 200), digitized with a 16-bit A/D converter (Digidata 1322A, Axon Instruments), and stored on a personal computer. Data acquisition and analysis were performed with pCLAMP 9 software. Curve fitting and statistical analysis were done with SigmaPlot and SigmaStat, respectively (Jandel Scientific). The data are presented as mean values \pm SE.

RESULTS

Cx26 and Cx30 are colocalized in transfected HeLa cells. To determine whether Cx26 and Cx30 interact, we generated clones of HeLa cells that stably expressed Cx26 or Cx30, using a puromycin-resistance vector. We then transfected the cloned HeLa cells expressing Cx30 with a G418 resistance vector containing Cx26, thereby obtaining bulk-selected cells that expressed both Cx30 and Cx26. Because some antibodies against these two connexins are known to cross-react (40), we screened antibodies against Cx26 or Cx30 and used the rabbit antiserum against Cx30 combined with the mouse monoclonal antibody against Cx26 (which were found to have no cross-

reactivity as described in MATERIALS AND METHODS) to double label these cells.

As shown in Fig. 1, the cloned cell lines expressing either Cx26 (Fig. 1A) or Cx30 (Fig. 1B) had gap junction plaques on apposed cell membranes composed solely of the expected connexin. We found similar results with multiple clones of cells expressing either Cx26 or Cx30 (data not shown). Furthermore, nearly all of the cells coexpressing Cx26 and Cx30 also had gap junction plaques on apposed cell membranes composed of both connexins that were largely colocalized (Fig. 1C). Cells transfected with an "empty" expression plasmid or parental HeLa cells were not labeled with either antibody (data not shown).

Cx26 and Cx30 coimmunoprecipitation. The colocalization of Cx26 and Cx30 in the cotransfected cells suggested that they could form heteromeric hemichannels. To evaluate this possibility, we performed coimmunoprecipitation experiments. We first investigated whether the antibodies identified in the above immunostaining experiments would cross-react on immunoblots. As shown in Fig. 2A, the mouse monoclonal antibody against Cx26 and rabbit antiserum against Cx30 that we used in our immunostainings did not cross-react, nor did a rabbit antiserum against Cx26. We then used the rabbit antiserum against Cx30 to immunoprecipitate lysates from clonal cell lines that stably expressed either Cx26 alone or Cx30 alone or bulk-selected cells that expressed Cx26 and Cx30 and blotted

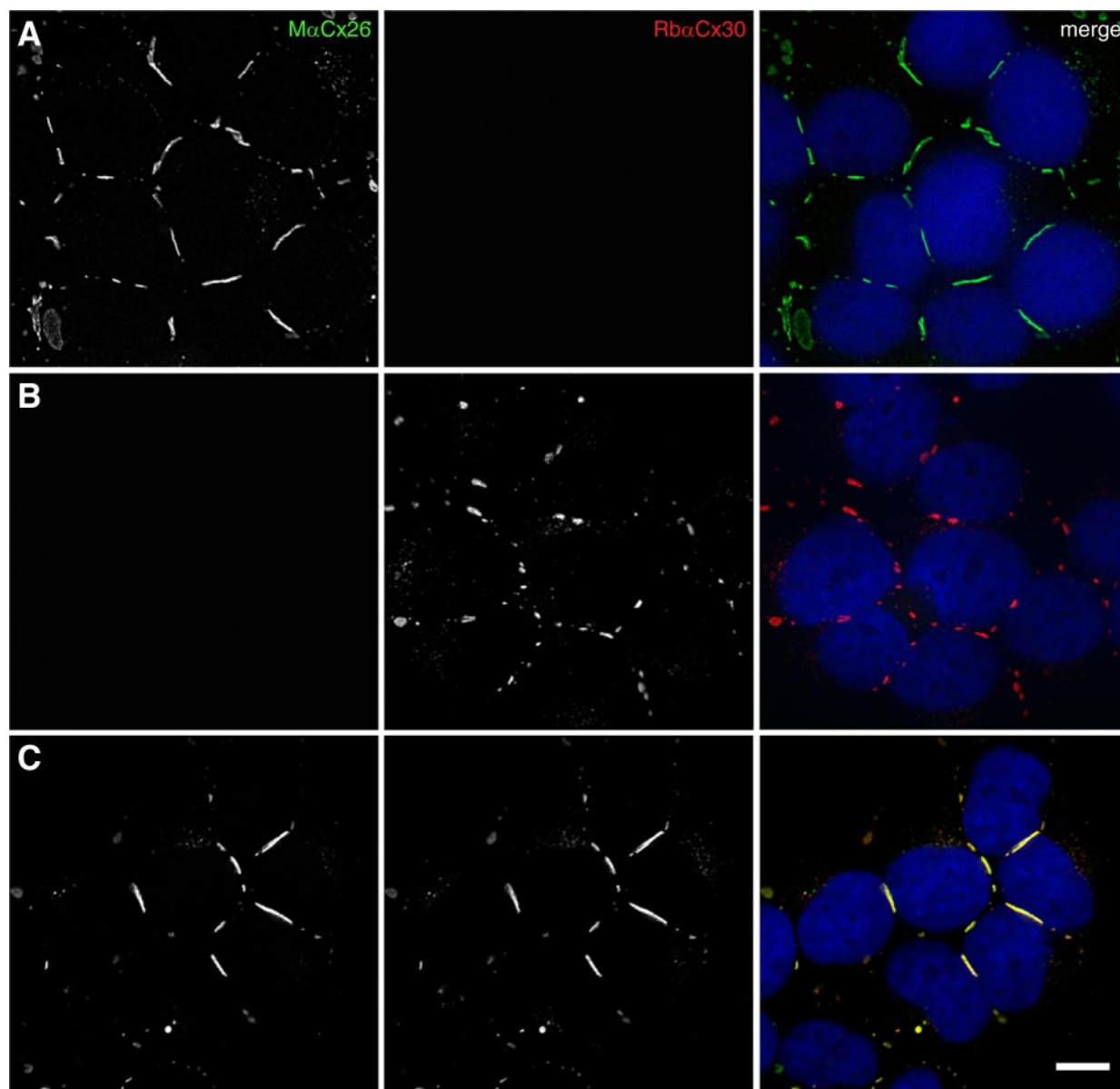


Fig. 1. Connexin26 (Cx26) and connexin30 (Cx30) are colocalized. These are deconvolved images of HeLa cells that stably express Cx26 (A), Cx30 (B), or Cx26 and Cx30 (C). Cells were colabeled with a mouse antibody against the COOH terminus of Cx26 (green) and a rabbit antiserum against the COOH terminus of Cx30 (red), as indicated and counterstained with DAPI (blue). Most of the Cx26 and Cx30 staining is found in gap junction plaques at the cell borders. Note that the Cx26 antibody did not cross-react with Cx30 and that the Cx30 antibody did not cross-react with Cx26. Cx30 and Cx26 are largely colocalized in cells that coexpress them (C). Scale bar = 10 μ m.

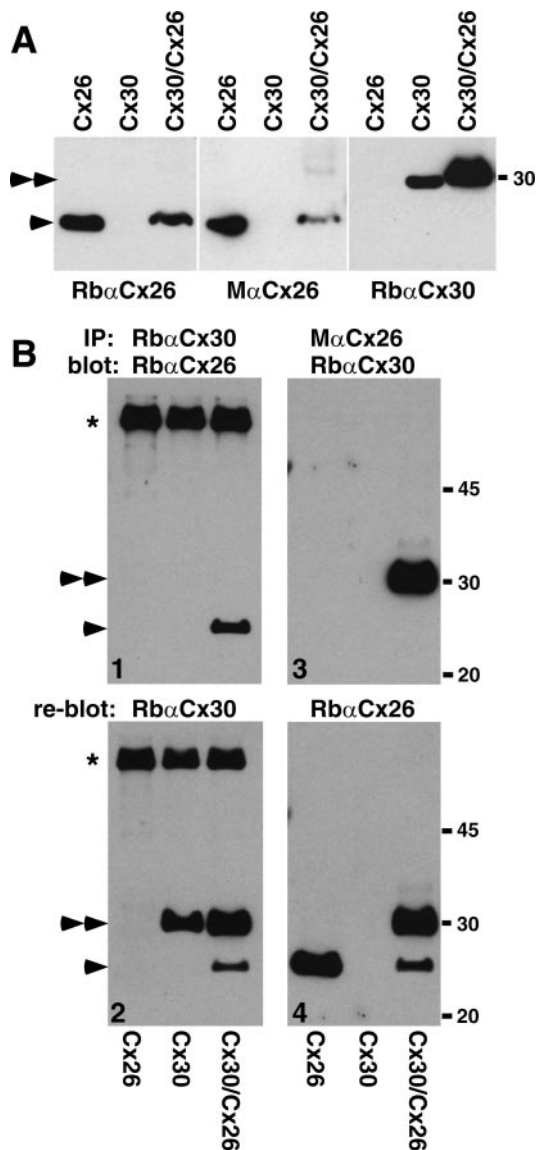


Fig. 2. Cx26 and Cx30 coimmunoprecipitates. *A*: immunoblots from HeLa cells that stably express Cx26 alone, Cx30 alone, or Cx26 and Cx30. Three blots were made and separately hybridized with a mouse monoclonal antibody against Cx26 ($M\alpha Cx26$), a rabbit antiserum against Cx26 ($Rb\alpha Cx26$), or a rabbit antiserum against Cx30 ($Rb\alpha Cx30$). Note that none of these antibodies show cross-reactivity between Cx26 and Cx30. *B*: cell lysates from HeLa cells that stably express Cx26, Cx30, or Cx30 and Cx26 were immunoprecipitated (IP) with $Rb\alpha Cx30$, probed with $Rb\alpha Cx26$ (1), and then reprobed with $Rb\alpha Cx30$ (2) or immunoprecipitated with $M\alpha Cx26$, probed with $Rb\alpha Cx30$ (3), and then reprobed with $Rb\alpha Cx26$ (4). Note that the $Rb\alpha Cx30$ coimmunoprecipitates Cx26 (1) and that the $M\alpha Cx26$ coimmunoprecipitates Cx30 (3). Because the blots were not stripped before reprobing them, the signal for Cx26 (single arrowhead) is still present in panel 2, and the signal for Cx30 (double arrowhead) is still present in panel 4. *Rabbit IgG used in the immunoprecipitation. Size markers (in kDa) are shown at right.

the immunoprecipitate with a rabbit antiserum against Cx26. As shown in Fig. 2*B*, left, a band corresponding to Cx26 (single arrowhead) was seen in the lysate from cells expressing both Cx26 and Cx30 but not in the other two lysates. Rehybridizing the blot with a rabbit antiserum against Cx30 demonstrated that Cx30 was present in lysates from cells expressing Cx30 alone and from cells expressing both Cx26 and Cx30.

We also performed the reciprocal experiment, using a mouse monoclonal antibody against Cx26 to immunoprecipitate lysates from these cells, and blotted the immunoprecipitates with a rabbit antiserum against Cx30 (Fig. 2*B*, right). A band corresponding to Cx30 (double arrowheads) was seen in the lysate from cells expressing both Cx26 and Cx30 (Fig. 2*B*) but not in lysates from cells expressing Cx26 or Cx30 alone. Rehybridizing the blot with a rabbit antiserum against Cx26 demonstrated that it was present in lysates from cells expressing Cx26 alone and from cells expressing both Cx26 and Cx30. To show that the interaction between Cx26 and Cx30 is specific, we repeated this experiment using cells that coexpressed Cx26 and Cx43, as the latter pair are not thought to interact (24). As shown in supplemental Fig. S.1, right, Cx43 (triple arrowheads) was found both in the crude lysate and in the unbound fraction but not in the bound fraction of the Cx26 immunoprecipitates of cells coexpressing Cx26 and Cx43. As in Fig. 2*B*, Cx30 was immunoprecipitated with Cx26 (supplemental Fig. S.1, left). These results demonstrate that Cx26 and Cx30 selectively interact.

Cx26 and Cx30 interact directly, as determined by u-af FRET. As an independent way to determine whether Cx26 and Cx30 interact, we used FRET, an imaging technique that can demonstrate the proximity of fluorescently tagged proteins to one another. FRET is thought to only occur between molecules separated by 10 nm or less (12, 65). Because the diameter of an entire hemichannel is ~ 7 nm (54), the individual subunits within a hemichannel should show FRET if they carry appropriate fluorophores. We adopted the method of acceptor-depletion FRET with linear spectral unmixing (16, 26) because it corrects for spectral bleeding through and provides relative concentrations of donor and acceptor fluorophores, thus allowing us to use the membrane clustering model (29, 30) to interpret our results. This model separates FRET signals arising from direct protein-protein interactions from those arising from random association. This model has been verified and used to interpret the formation of molecular complexes in the plasma membrane and ER, including connexin molecules (16, 26, 31, 46, 67). In this model, for proteins that directly interact, FRET increases as the D-A ratio decreases and is not correlated with the absolute level of the acceptor. In contrast, for proteins that interact only by random association, FRET does not correlate with the D-A ratio but increases with the absolute level of the acceptor. Proteins are considered partially clustered when FRET increases as the D-A ratio decreases and with the increase of absolute level of the acceptor.

FRET was performed on cells that were cotransfected with different combinations of Cx26-ECFP, Cx26-EYFP, Cx30-ECFP, Cx30-EYFP, and Cx43-EYFP. Cells coexpressing Cx26-ECFP/Cx26-EYFP or Cx30-ECFP/Cx30-EYFP and Cx26-ECFP/Cx43-EYFP were used as positive (16, 26) and negative (24) controls, respectively. For each group of cells that were analyzed, several ROIs showing expression of both ECFP and EYFP were selected from the cytoplasm or the cell membrane. As shown in Fig. 3, FRET efficiency increased inversely with the D-A ratio in cells coexpressing Cx30-ECFP and Cx26-EYFP. The FRET observed in ROIs from the cell membrane (including gap junction plaques) was similar to that in the cytoplasm (supplemental Fig. S.3). Because FRET efficiency also increased with the A-level, our result fits the

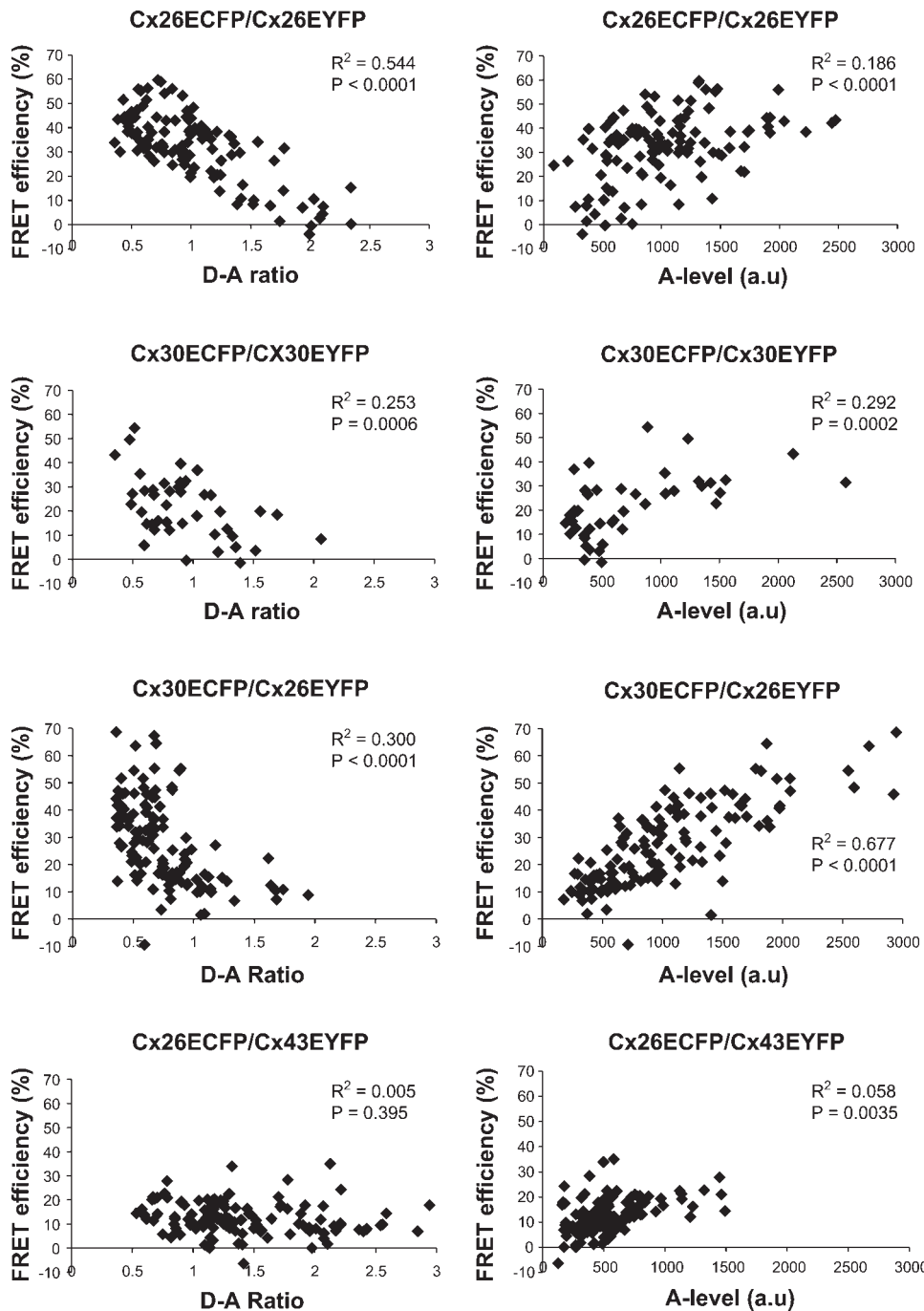


Fig. 3. Cx26 and Cx30 interact directly, determined by acceptor depletion fluorescence resonance energy transfer with linear spectral unmixing (u-ad FRET). The mean FRET efficiency is plotted as a function of relative concentration ratio of donor to acceptor (D-A ratio) or acceptor emission level [A-level, in arbitrary units (au)] for different combinations of connexins. In cells coexpressing Cx26ECFP/Cx26EYFP, Cx30ECFP/Cx30EYFP, or Cx30ECFP/Cx26EYFP, the FRET efficiency increased inversely with the D-A ratio, indicating that the donors and acceptors directly interact in molecular complexes, likely because at least some of them form heteromeric connexons. Because FRET efficiency also increased with the A-level, some interactions between the donor and acceptor are likely to be by random association. In contrast, the FRET efficiency of cells coexpressing Cx26ECFP/Cx43EYFP was independent of the D-A ratio but increased with the A-level, indicating that Cx26ECFP and Cx43EYFP did not interact directly. Each symbol represents 1 region of interest.

partially clustered model, suggesting that Cx30 and Cx26 interact in molecular complexes, which are likely to be at least in part heteromeric connexons. The nature of the random association is unknown but is also found in cells expressing Cx26 or Cx30 alone. In contrast, in cells coexpressing Cx26-ECFP and Cx43-EYFP, FRET efficiency was not correlated with the D-A ratio but increased with A-level, consistent with the random association model. Our FRET data for Cx26 and Cx30 compare well with those of Di et al. (16), who did not, however, analyze cells coexpressing two connexins that do not form heteromers.

The result of our negative control indicates that FRET between Cx26-EYFP and Cx30-ECFP in cells coexpressing

them are specific. Although we are unaware of any direct measurements on the lengths of the COOH termini for either Cx26 or Cx30, the structure of green fluorescent protein has been determined (the "barrel" is 2.4 nm \times 4.2 nm; Ref. 41). In freeze-fracture electron microscopy under some conditions, individual hemichannels can appear to be tightly packed in a hexagonal lattice (Fig. 97 in Ref. 21), raising the possibility that connexins in adjacent hemichannels could interact. Whether this could occur in our transfected cells is unknown because we have no independent way to determine the distance between adjacent hemichannels in the living cell, and gap junctions in biological membrane are usually not tightly packed (Fig. 100 in Ref. 21). Because of these uncertainties,

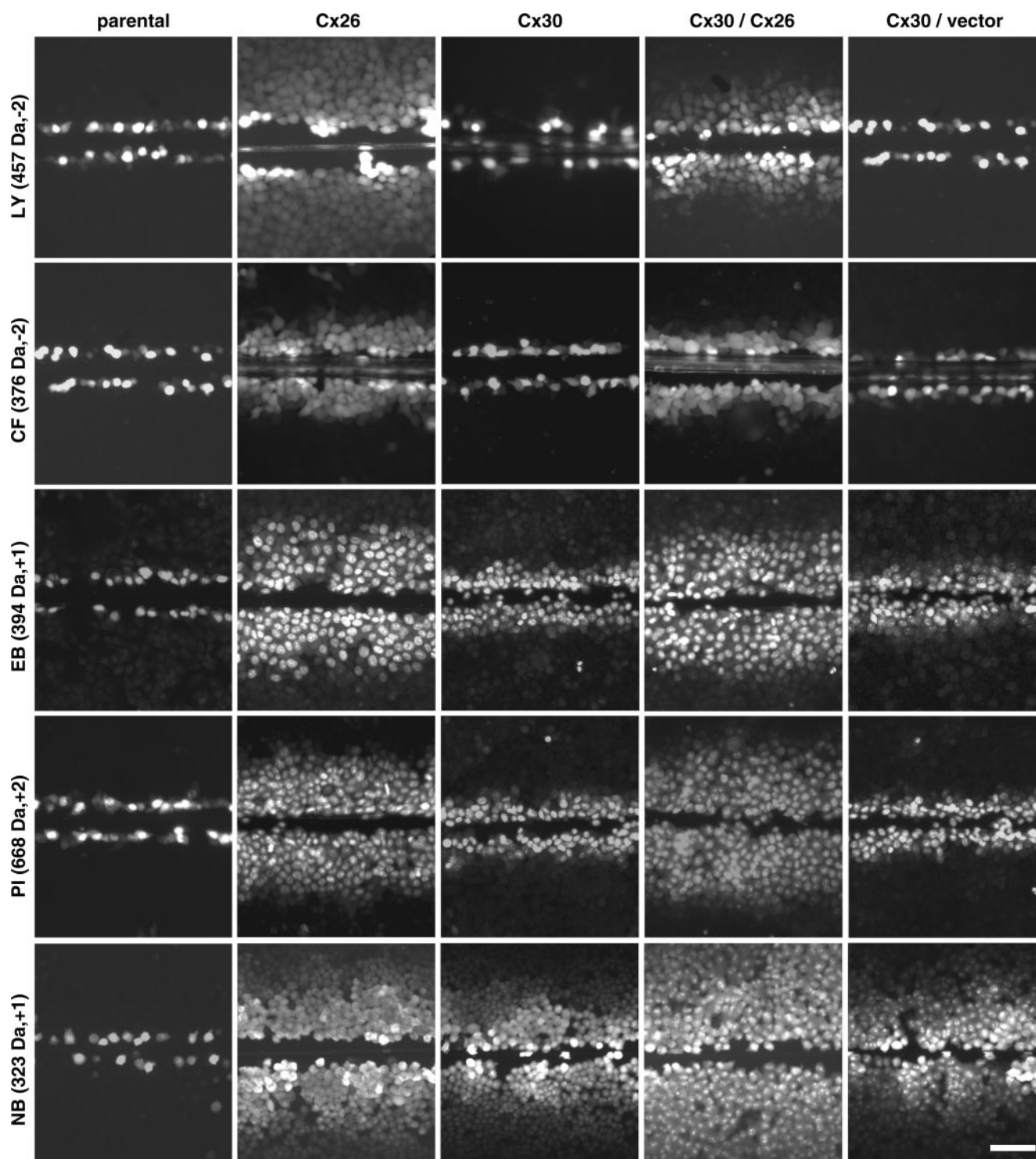


Fig. 4. Dye transfer after scrape loading cells that stably express Cx30 and/or Cx26. These are digital fluorescence images of confluent cloned HeLa cells that stably express Cx26 or Cx30, bulk-selected cells that express both Cx30 and Cx26 (Cx30/Cx26), Cx30 and an "empty" vector (Cx30/vector), or parental HeLa cells. Cells were incubated in 0.1% Lucifer yellow (LY), 1 mM 5,6-carboxyfluorescein (CF), 0.1% ethidium bromide (EB), 0.3% propidium iodide (PI), or 2% neurobiotin (NB; visualized with fluorescently conjugated avidin) and imaged ~15 min after being wounded with a scalpel blade. The wounded cells picked up the dye in all cases, but there was no transfer of dye from wounded parental cells to neighboring cells. Wounded cells that expressed Cx26 alone or both Cx26 and Cx30, in contrast, showed transfer of all dyes. Wounded cells that expressed Cx30 alone or Cx30 plus empty vector showed transfer of NB, EB, or PI but not LY or CF. Scale bar = 100 μ m.

we performed an important negative control in cells coexpressing two connexins that are known not to form hemichannels (Cx26 and Cx43).

Functional analysis of cells expressing Cx26 and/or Cx30. To investigate the functional properties of channels coassembled from Cx26 and Cx30, we performed scrape loading on bulk-selected cells coexpressing Cx30 and Cx26. We compared these cells to clonal cell lines stably expressing Cx26 or Cx30, parental HeLa cells, and bulk-selected cells coexpressing Cx30 and empty vector (pIRESneo3). In this assay (20), monolayers of cultured cells were cut with a scalpel blade in the presence of gap junction-permeant dyes. We used fluorescent molecules of differing size and charge: LY (457 Da, -2 charge), CF (376 Da, -2 charge), EB (394 Da, $+1$ charge), and PI (668 Da, $+2$ charge), as well as a nonfluorescent tracer (NB; 323 Da, $+1$), which can be visualized with fluorescently conjugated avidin. We quantified the extent of dye transfer by measuring the distance from the scrape line to the point where the fluorescence intensity dropped to $1.5 \times$ the background fluorescence intensity. As shown in Fig. 4 and quantified in Fig. 5 and Table 1, none of these tracers diffused beyond the wounded parental cells, confirming that they are communication incompetent. Three different clonal cell lines stably expressing Cx26 robustly transferred all the tracers; examples from one cell line are shown. In contrast, three different clonal cell lines stably expressing Cx30 transferred EB, PI, and NB (all positively charged) but not LY or CF (both negatively charged); examples from one cell line are shown. Cells expressing Cx26 were more permeant to EB and PI (~ 2 -fold) than cells expressing Cx30. Bulk-selected cells coexpressing Cx30 and Cx26 transferred all tracers, but LY and CF did not appear to diffuse as far as in cells expressing Cx26 alone. On the other hand, cells expressing both Cx26 and Cx30 spread PI and NB further than cells expressing Cx26 or Cx30 alone, whereas bulk-selected cells that express both Cx30 and the empty vector used to express Cx26-transferred tracers such as cells expressing Cx30 alone. These findings demonstrate that homotypic Cx26 and homotypic Cx30 channels have different permeability properties and suggest that the gap junctions formed by cells that coexpress both Cx26 and Cx30 have "emergent" permeation properties; that is, they are more permeable to NB. This argument assumes that all cells express about equal numbers of functioning channels, which was not simultaneously determined in these experiments, but is consistent with the electrophysiological data presented below (Table 3). To exclude the possibility of dye passage from cell to cell through other mechanisms such as cytoplasmic bridges, we also scrape loaded cells with the gap junction-impermeant 10,000-Da tetramethylrhodamine dextran, which was confined to the scrape-loaded cells in all of the cell lines (data not shown).

To investigate further the comparative permeability of these connexin channels, we compared FRAP, a quantitative analysis of dye transfer, results. FRAP could only be performed for calcein (623 Da; -4 charge), a negatively charged dye that has a cell-permeant counterpart (calcein-AM) that is cleaved within cells; we could not find an esterified version of a positively charged dye. Confluent monolayers of clonal cells stably expressing Cx26 or Cx30 or bulk-selected cells that express both Cx30 and Cx26 or Cx30 and the empty vector used to express Cx26 were incubated in calcein-AM. Individ-

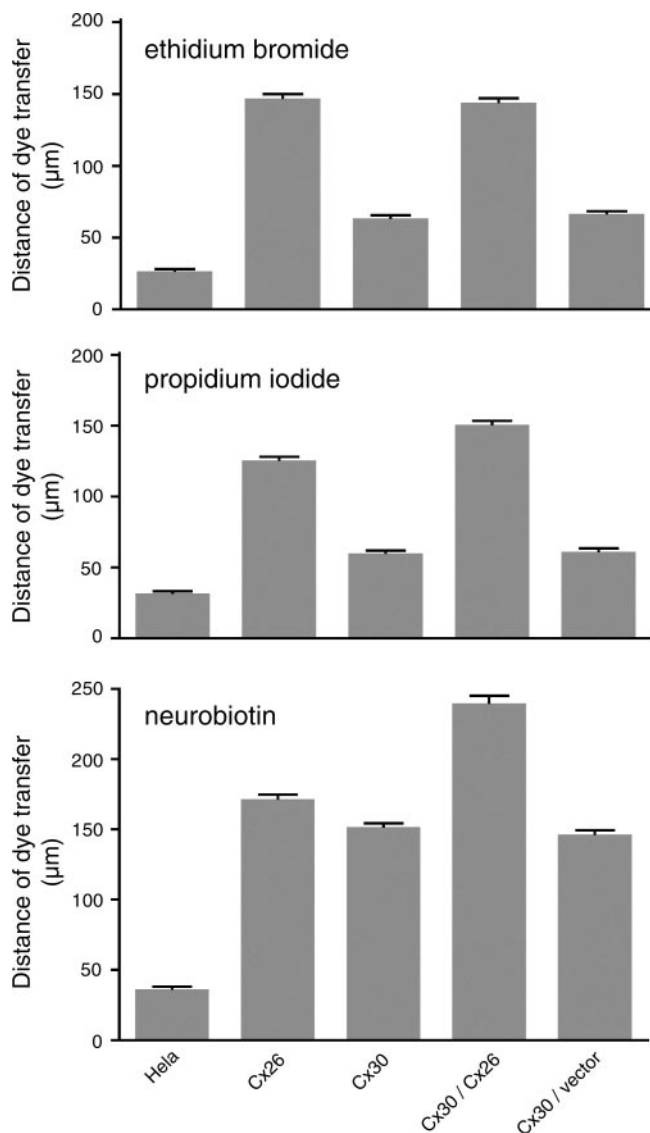


Fig. 5. Quantitative analysis of intercellular dye transfer after scrape loading. The columns represent the mean distance of dye transfer from the scrape line to the point where the fluorescence intensity dropped to $1.5 \times$ the background intensity. For each cell line, this was measured for the indicated dyes, by acquiring at least 8 images from each of 3 different plates of cells. Error bars indicate \pm SE.

ual cells that were in close contact with at least four surrounding cells were photobleached for 600 ms, avoiding bleaching of the adjacent cells. Images were acquired immediately before and after bleaching and every 10 s thereafter for 500 s (typical examples are shown in Fig. 6A). Fluorescence was measured as mean pixel density in the bleached cells in every image.

For each cell line, we analyzed between 11 and 28 individual cells, normalizing the data by assigning the fluorescent signal present in each cell immediately before and immediately after photobleaching as 100% and 0%, respectively. These results are shown in Fig. 6B, which depicts the mean percent recovery plotted against time postbleaching; the vertical bars represent mean values \pm SE. Cells expressing Cx26 alone (presumably homotypic Cx26 channels) had a rapid FRAP, recovering 50% of their prebleach signal after just 30 s. Cells expressing Cx30

Table 1. Comparison of intercellular dye transfer after scrape-loading cells that stably express Cx30 and/or Cx26

Cell Line	Distance, μm	P Value			
		Cx26	Cx30	Cx30/Cx26	Cx30/vector
<i>Ethidium bromide</i>					
HeLa	27.1 \pm 1.0 (n=36)	<0.001	<0.001	<0.001	<0.001
Cx26	147 \pm 2.7 (n=32)		<0.001	>0.05	<0.001
Cx30	64.1 \pm 1.5 (n=33)			<0.001	>0.05
Cx30/Cx26	145 \pm 2.6 (n=31)			<0.001	
Cx30/vector	67.2 \pm 1.3 (n=30)				
<i>Propidium iodide</i>					
HeLa	32.1 \pm 1.2 (n=26)	<0.001	<0.001	<0.001	<0.001
Cx26	126 \pm 2.0 (n=33)		<0.001	<0.001	<0.001
Cx30	60.6 \pm 1.4 (n=30)			<0.001	>0.05
Cx30/Cx26	151 \pm 2.2 (n=28)				<0.001
Cx30/vector	61.6 \pm 1.9 (n=36)				
<i>Neurobiotin</i>					
HeLa	36.7 \pm 1.3 (n=30)	<0.001	<0.001	<0.001	<0.001
Cx26	172 \pm 2.7 (n=40)		<0.001	<0.001	<0.001
Cx30	152 \pm 2.3 (n=31)			<0.001	>0.05
Cx30/Cx26	240 \pm 4.8 (n=33)				<0.001
Cx30/vector	147 \pm 2.5 (n=33)				

The distance (means \pm SE) is calculated from the scrape line to the point where the fluorescence intensity dropped to 1.5 \times the background intensity. Cx, connexin.

alone or Cx30/pIRES (presumably homotypic Cx30 channels) had a very slow FRAP, recovering only \sim 15% of their prebleach signal after 500 s, which was, nevertheless, detectably greater than that in parental cells, which recovered only 4% after 500 s. Cells expressing both Cx26 and Cx30 (presumably heteromeric and heterotypic channels of Cx26 and Cx30) recovered 50% of their prebleach signal after 165 s, intermediate between that of cells expressing Cx26 alone and cells expressing Cx30 alone. To ensure that our FRAP results were not caused by the reentry of calcein-AM from the solution or by the spontaneous recovery of fluorescence, we also bleached individual cells that were not in contact with any other cells. Fluorescence did not return in bleached isolated cells (data not shown). For statistical analysis, regression model with autocorrelated errors was applied to obtain a fit for the recovery curves over time, and three parameters in the model (coefficients of quadratic term and linear term of time, as well as the constant term) between two cell lines were compared. These curves were significantly different among all of the cell lines ($P < 0.0001$), except for those between Cx30 and Cx30/vector, as shown in Table 2.

FRAP analysis of homotypic Cx26, homotypic Cx30, and heterotypic Cx26-Cx30 coupling. Because Cx26 and Cx30 are coexpressed in the cochlea, we wished to determine whether these two connexins could form heterotypic channels that pass calcein. By modifying our FRAP assay, we developed a way to perform this analysis, which is conceptually similar to the "preloading" assay described by Abraham et al. (1). One cell type (clonal cell lines stably expressing Cx26 or Cx30) was prelabeled with DiI and cocultured with unlabeled cells at 1:30. After 24–30 h in coculture, the cells were incubated with calcein-AM, and individual DiI-labeled cells (which were in close contact with at least 4 non-DiI-labeled cells) were bleached and analyzed by FRAP as described above. To minimize phototoxicity to the cells, DiI was not bleached, and

the laser used to detect the DiI signal was turned off after the prebleaching image was obtained. We analyzed between 25 and 46 individual cells in each combination of cocultured cells.

When DiI-labeled cells expressing Cx26 were cocultured with cells expressing Cx26, FRAP was robust, recovering 50% of their prebleach signal after just 35 s (Fig. 6D), as in our prior analysis (Fig. 6B). When DiI-labeled cells expressing Cx30 were cocultured with cells expressing Cx30, FRAP was very slow, recovering only 13% after 500 s (Fig. 6D), as in our prior analysis (Fig. 6B). Coculturing DiI-labeled cells expressing Cx26 with cells expressing Cx30 or, conversely, coculturing DiI-labeled cells expressing Cx30 with cells expressing Cx26 both showed an intermediate degree for FRAP (Fig. 6D), recovering 47% and 41% after 500 s, respectively. These results are summarized in Fig. 6D, which depicts the mean percent recovery plotted against time postbleaching; the vertical bars represent means \pm SE. These recovery curves were significantly different statistically among the four cell pairs ($P < 0.0001$), as shown in Table 2.

Electrophysiological characterization of gap junction channels in cells expressing Cx26 and/or Cx30. Gap junctional currents in pairs of HeLa cells transfected with Cx26 and/or Cx30 were analyzed by the double whole cell patch-clamp technique. Analysis of these cell pairs showed considerable electrical coupling via gap junctions. To distinguish between gap junctions and cytoplasmic bridges, the preparations were treated by exposure to CO₂ (56), which abolishes intercellular currents due to gap junctions but does not affect cytoplasmic bridges. Table 3 summarizes the total junctional conductance and single-channel conductance in different cell pairs investigated. The mean macroscopic conductance between homotypic cell pairs expressing Cx26 and Cx30 was 8.4 and 12.7 nS, respectively. Division of these macroscopic coupling data by the single-channel conductance values for Cx26 (95 pS) and Cx30 (135 pS)

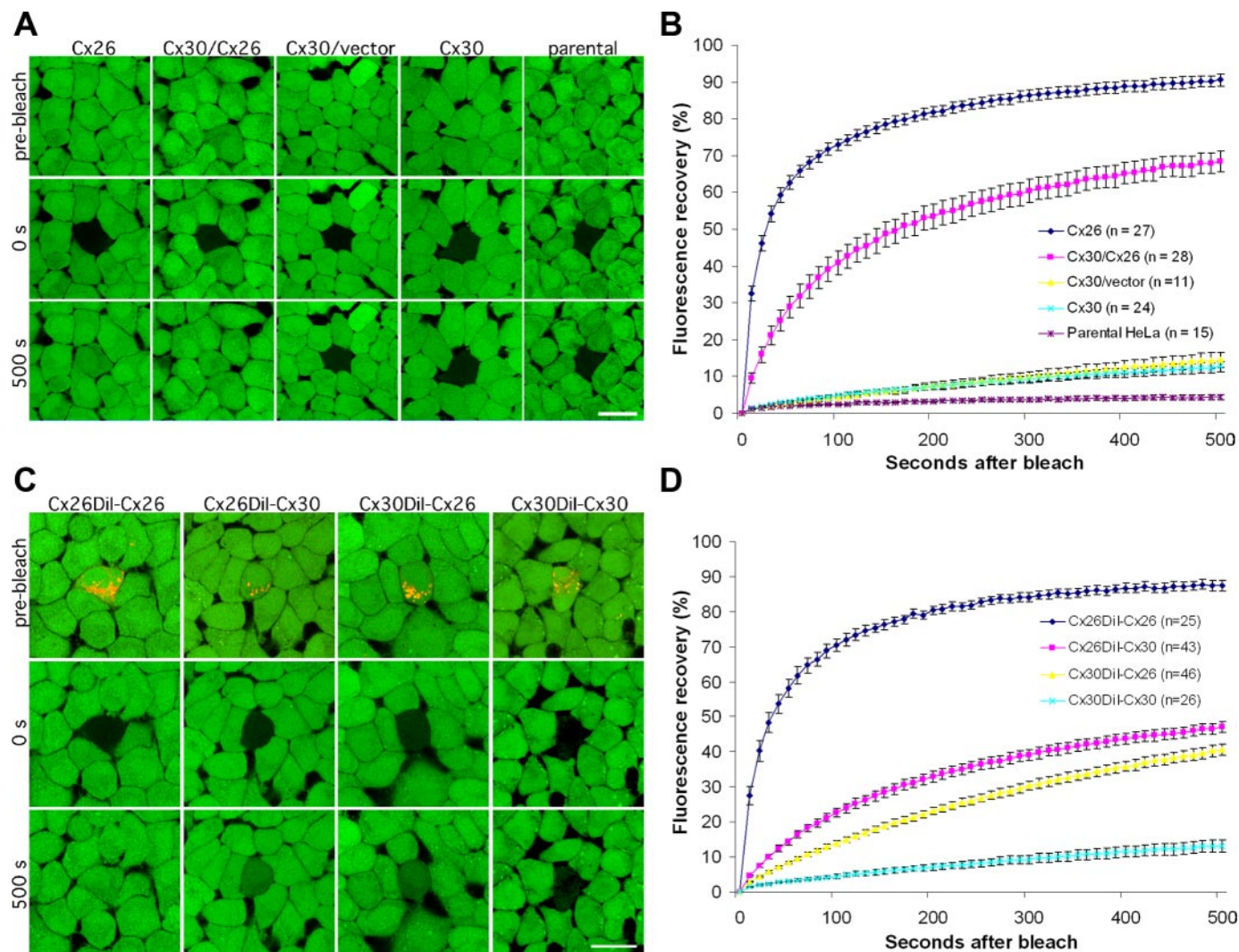


Fig. 6. Fluorescence recovery after photobleaching (FRAP) analysis of Cx26 and/or Cx30 gap junction channels. HeLa cells stably expressing Cx26, Cx30, or both (A and B) were incubated in calcein-AM to fill the cytoplasm with calcein (green). Selected cells were photobleached, and the green fluorescence signal was measured every 10 s for 500 s. For analysis of heterotypic Cx30 and Cx26 gap junction channels (C and D), cells stably expressing Cx26 or Cx30 were prelabeled with DiI (a red dye that labels cell membranes) and mixed with unlabeled cells stably expressing either Cx26 or Cx30, at a ratio of 1:30. After 24–30 h of coculture, cells were incubated in calcein-AM, and individual DiI-positive cells surrounded by nonDiI-labeled cells were selected for photobleaching and monitored for recovery of green fluorescence as described above. A and C: examples of cells immediately (10 s) before, immediately after (0 s), and 500 s after bleaching. C and D: summarized data for many cells, by normalizing the fluorescent signal present in each cell immediately before and immediately after photobleaching to 100% and 0%, respectively. The curves connect the mean percent recovery at each time point; the vertical bars represent means \pm SE. Note that the calcein signal recovers in the bleached cells expressing Cx26 or both Cx26 and Cx30 (Cx30/Cx26) but not in the bleached cells expressing Cx30, Cx30, and empty vector (Cx30/vector) or in parental HeLa cells (A and B). In cells coupled by Cx26-Cx30 heterotypic channels (Cx26DiI-Cx30 and Cx30DiI-Cx26), the rate of recovery of the calcein signal is intermediate between their homotypic counterparts (C and D). Scale bars = 20 μ m.

yielded an estimate of \sim 90 functioning channels between each type of homotypic cell pair on average.

The relationship between V_j and junctional conductance was also studied in cell pairs expressing various combinations of Cx30 and/or Cx26. The junctional currents observed in homotypic Cx30 cell pairs exhibited significant time and voltage dependence (Fig. 7A), similar to that reported for mouse Cx30 (57). In contrast, the junctional currents in Cx26 cell pairs (Fig. 7B) showed little if any V_j dependence, typical of homotypic Cx26 channels (24, 58). The voltage-dependent behavior of the macroscopic junctional currents in heterotypic Cx26-Cx30 cell pairs appeared intermediate between the behaviors of homotypic Cx26 and Cx30 channels. Some heterotypic cell pairs demonstrated moderate voltage dependence (Fig. 7C, left);

other cell pairs showed stronger V_j gating when the Cx26 side was negative or the Cx30 side was positive (Fig. 7C, right). Rectification and activation of gap junction currents are features of heterotypic channels that have been shown previously (56, 60) and may reflect heterotypic channels composed from connexins with opposite gating polarities. The currents observed in pairs coexpressing Cx26/Cx30 (Fig. 7D) exhibited a complex voltage dependence ranging from significant sensitivity to V_j (Fig. 7D, top left) to virtually insensitive examples (Fig. 7D, top right), with additional intermediate and/or asymmetrical V_j dependence in other pairs (Fig. 7D, bottom). Moreover, in some cell pairs, the currents closely resembled those of homotypic Cx26 or homotypic Cx30 channels. Such behavior is expected when the two coexpressed connexins have distinct

Table 2. Statistical analysis comparing FRAP between specific cell lines

Cell Line	P Value							
	Cx30	Cx26	Cx30/ Vector	Cx30/Cx26	Cx26DiI-Cx26	Cx26DiI-Cx30	Cx30DiI-Cx26	Cx30DiI-Cx30
HeLa parental	<0.0001	<0.0001	<0.0001	<0.0001				
Cx30		<0.0001	0.172	<0.0001				0.828
Cx26				<0.0001	0.304			
Cx30/vector				<0.0001				0.447
Cx30/Cx26						<0.0001	<0.0001	
Cx26DiI-Cx26						<0.0001	<0.0001	<0.0001
Cx26DiI-Cx30							<0.0001	<0.0001
Cx30DiI-Cx26								<0.0001

FRAP, fluorescence recovery after photobleaching. To determine whether the slope of the curves differed from each other in cells expressing variable combinations of Cx26 and/or Cx30, regression model with autocorrelated errors was applied to model recovery curve over time using the SAS software version 9.1, and the 3 parameters in the model (coefficients of quadratic term and linear term of time, as well as the constant term in the formula) between 2 cell lines were compared. $P < 0.05$ was considered to be significant.

sensitivities because the junctional current profile depends on the expression level of the two connexins, i.e., variations in the protein ratio of Cx26 and Cx30 in different cell pairs and thus the corresponding ratio of homotypic, heterotypic, and heteromeric channels formed (56).

Weakly coupled cell pairs were selected to study single gap junction channel currents. Figure 8A shows records from one operational channel obtained from a homotypic Cx30 cell pair at different V_j values. The currents yielded conductances of the main and residual states of 133–142 pS and 14–24 pS, respectively. The range of main state unitary conductances recorded from homotypic Cx30 pairs was 120–150 pS (Table 3). These unitary channel conductances closely correspond to the sizes of homotypic mouse Cx30 channels reported previously under the same experimental conditions (57). In Fig. 8A, as V_j increased from 50 mV (top) to 70 mV (middle) and 90 mV (bottom), channels spent less time in the main open state and more time in the residual state. However, substate activity was prominent for Cx30 homotypic channels particularly at higher V_j values. At 90 mV (Fig. 8A, bottom), channels spent only a brief time in the main state conductance of ~140 pS and then only reached a current level corresponding to 60-pS conductance, which presumably reflects a channel substate. Microscopic currents recorded from homotypic Cx26 cell pairs (Fig. 8B) showed typical single-channel events with unitary conductances of 100–110 pS induced only at much higher voltage ($V_j = 90$ mV) compared with Cx30. A residual state was largely absent for homotypic Cx26 channels. Such single-channel conductances and V_j gating correspond to mouse Cx26 channels reported under the same experimental conditions (58).

Microscopic currents obtained from heterotypic Cx26-Cx30 cell pairs showed conductance and gating properties intermediate between homotypic Cx26 and Cx30 channels. Figure 9 shows examples of current records from heterotypic cell pairs with one operational channel. Similar to homotypic Cx30 channels, but not homotypic Cx26 channels, higher V_j (80 mV) induced heterotypic Cx26-Cx30 channel gating from fully open main states to lower conductance substates. When the voltage was altered in the Cx30-expressing cell (Fig. 9, A and C) or in the Cx26 expressing cell (Fig. 9B), single-channel currents measured in the Cx26 expressing cell or the Cx30 expressing cell, respectively, yielded main state unitary conductances from 105 to 130 pS (Table 3), with occasional

residual state conductances of 13–28 pS. Although the heterotypic channel unitary conductance did not show apparent voltage polarity dependence, polarity-dependent channel gating was clearly shown in some records. When the Cx30 cell was made relatively negative, by hyperpolarizing the Cx30 cell or by depolarizing the Cx26 cell, the heterotypic Cx26-Cx30 channels remained in the main state for longer times; when the Cx30 cell was made relatively positive, the heterotypic Cx26-Cx30 channels tended to remain closed or in a residual state or substate (Fig. 9). Such single-channel behavior may explain the rectifying macroscopical current behavior recorded in some heterotypic pairs (Fig. 7C).

Single-channel currents from cell pairs coexpressing Cx26 and Cx30 yielded a broader spectrum of channel conductances. Figure 10 represents examples of currents with single-channel events recorded from doubly transfected Cx26/Cx30 cell pairs. These cells primarily contained events of three sizes: ~50–60, 80–110, and ~120–150 pS. The 80- to 110-pS and 120- to 150-pS groups could correspond to homotypic Cx26 and Cx30 channels, respectively, because events with such conductances were recorded from these cell pairs (Figs. 8), but the distribution of unitary conductances of heterotypic Cx26-Cx30 channels also overlaps these two groups. The 50- to 60-pS channel group may be a novel conductance, reflecting heteromeric Cx26/Cx30 channels, but we cannot exclude the possibility that it reflects substate conductances of homotypic Cx30 or heterotypic Cx26-Cx30 channels or transitions between substates (see Fig. 8A, bottom, for comparison). All cell pairs occasionally contained some small conductance events

Table 3. Electrophysiological data obtained from different types of HeLa cell pairs

Cell Pair Type	No. of Cell Pairs	Total Gap Junction Conductance, nS	Main Single-Channel Unitary Conductance, pS
Cx30-Cx30	27	12.7 ± 9.5	120–150
Cx26-Cx26	15	8.4 ± 6.3	80–110
Cx26-Cx30	12	15.3 ± 15	105–130
Cx26/30-Cx26/30	41	14.5 ± 8.9	50–60 80–110 120–150

Total junctional conductance values are means ± SD. Cell pairs consisting of different types of cells were examined for total gap junctional conductance and unitary conductance.

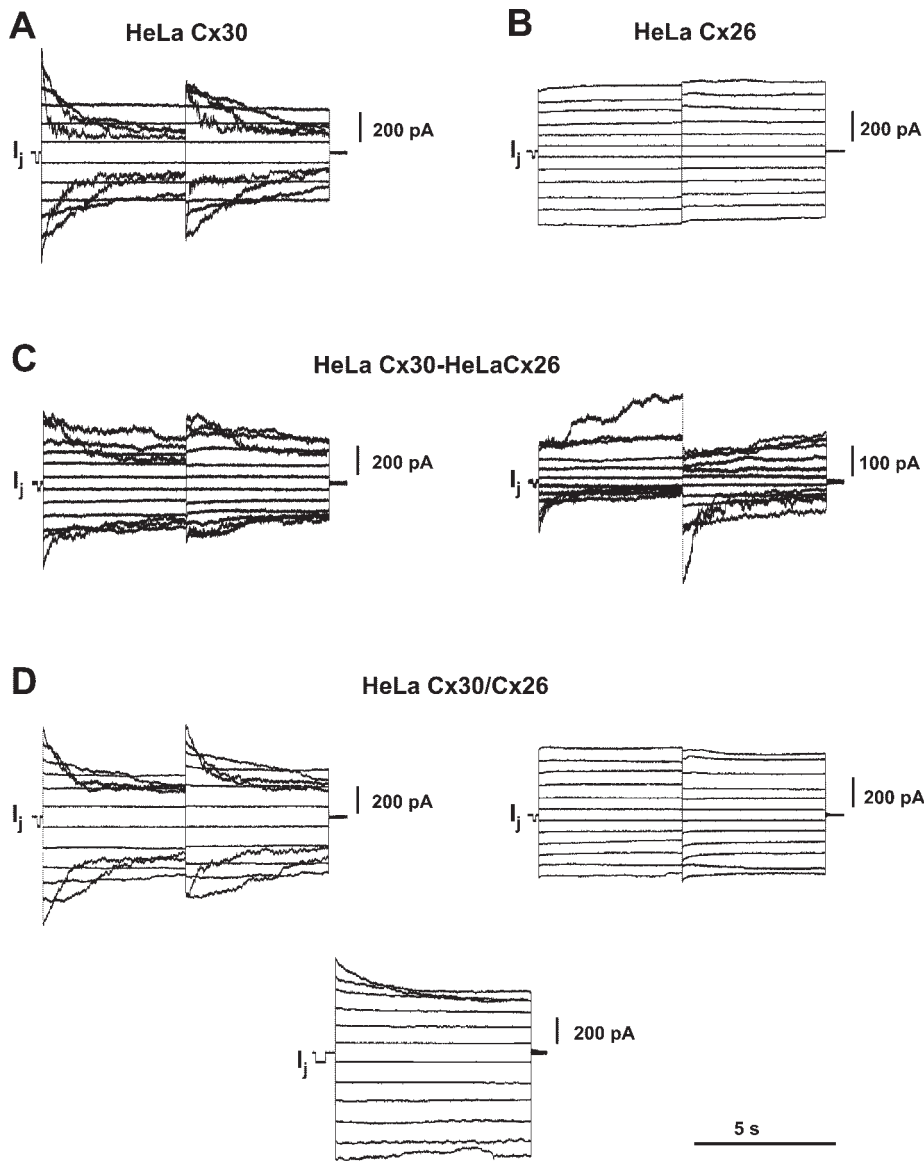


Fig. 7. Dependence of intercellular coupling on transjunctional voltage (V_j). Gap junction currents (I_j) were elicited by bipolar pulse protocol from different HeLa cell pairs by double whole cell patch clamping: homotypic Cx30 (A), homotypic Cx26 (B), heterotypic Cx26-Cx30 (C), and co-transfected Cx26/Cx30 (D). The voltage of 1 cell was changed in 20-mV steps from -110 to $+110$ mV, and I_j was measured in the other cell. I_j was voltage and time dependent in homotypic Cx30 but not in homotypic Cx26 cell pairs, intermediate between the behaviors of homotypic Cx26 and homotypic Cx30 channels in heterotypic Cx26-Cx30 cells pairs, and variable in Cx26/Cx30 co-expressing cell pairs.

(~ 25 – 30 pS, see Fig. 8B) that presumably correspond to endogenous HeLa cell channels (i.e., Cx45) (17, 18, 27, 60). Coexpression of two connexins could hypothetically produce 196 distinct heteromeric conductance states. Although the channel types shown may not be the only ones present in coexpressing cells, they represent examples of what was observed in multichannel and single-channel recordings and are consistent with the possibility of heteromeric channel formation.

DISCUSSION

Cx26 and Cx30 form heteromers. Our results confirm and extend previous reports that Cx26 and Cx30 form gap junction plaques when expressed individually (5, 14, 37–39, 49, 51, 52) and are colocalized in the same gap junction plaques when expressed together in cells (39, 49). Cx26 and Cx30 have also been coimmunoprecipitated from mouse cochlea or from transfected cells (2, 16, 22, 49), but ours is the first demonstration that untaged human Cx26 and Cx30 can be reciprocally

coimmunoprecipitated from transfected cells. In addition, our FRET data indicate that Cx26 and Cx30 directly interact (16, 26), whereas Cx26 and Cx43 do not form heteromers (24) by coimmunoprecipitation assay and by FRET. Finally, the channels in cells coexpressing Cx26 and Cx30 have distinct electrophysiological characteristics from those in cells expressing Cx26 or Cx30 alone. Together, these data indicate that human Cx26 and Cx30 specifically interact, likely by coassembling into heteromeric connexons.

Different gap junction channels have different permeabilities. We compared the permeability of gap junction channels composed of Cx26 or Cx30 by scrape loading, revealing that homotypic Cx26 channels were permeable to both cationic and anionic tracers, whereas homotypic Cx30 channels were permeable to cationic but not anionic tracers. The charge selectivity of Cx30 channels appeared to be independent of mass, as LY and EB have similar molecular weights, but opposite charges. Our results are consistent with previous studies in which tracers were injected into single cells (5, 19, 37, 39, 49),

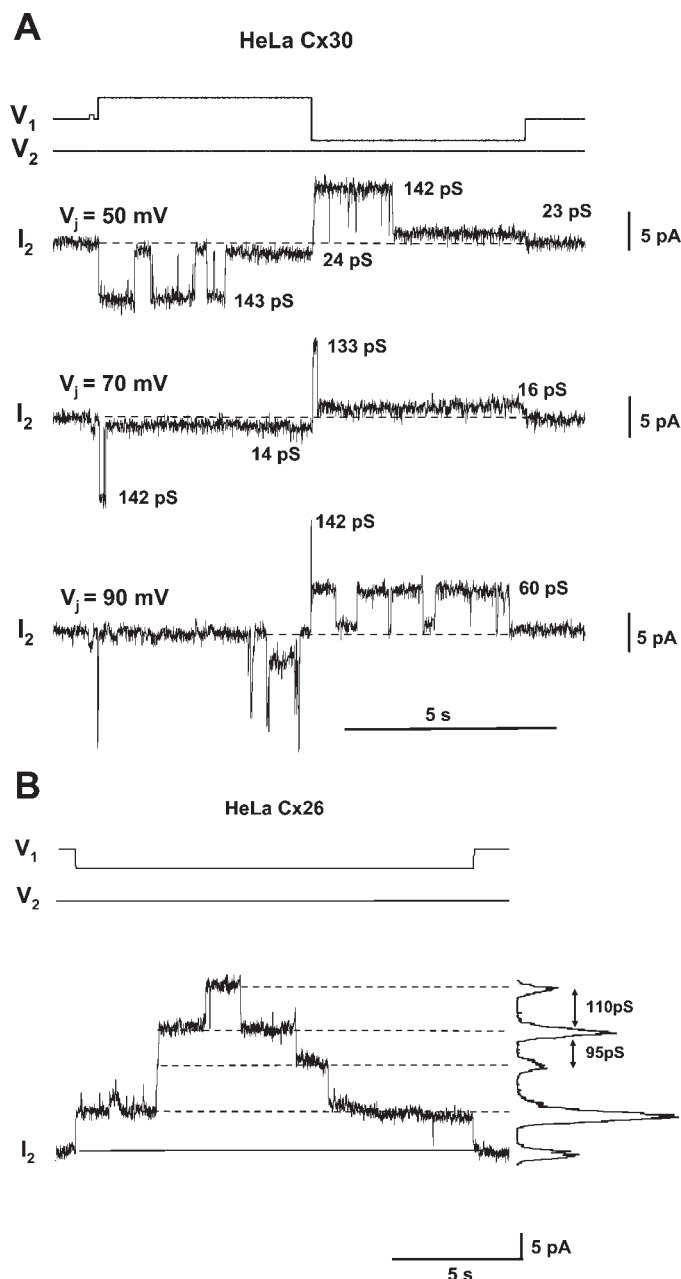


Fig. 8. Single-channel properties of homotypic Cx30 or homotypic Cx26 gap junction channels. *A*: bipolar pulse protocol (V_1 and V_2) and associated single-channel currents (I_2) recorded from a Cx30 cell pair with a single operational channel at different V_j values. When V_j was increased from 50 to 70 to 90 mV (top to bottom), the channel spent less time in the main state and more time in the residual state. Currents yielded main γ_j of 133 pS to -143 pS and residual γ_j of 14–24 pS, respectively (where γ_j is single-channel conductance). At $V_j = 90$ mV (bottom), the channel exhibited an intermediate current level between the main and residual and/or closed state, i.e., a substate with substate γ_j of 60 pS. Dashed lines correspond to a zero current level. *B*: multichannel recording obtained from a Cx26 cell pair at $V_j = 90$ mV. Solid line represents the zero current level, and dashed lines represent discrete current steps indicative of opening and closing of channels. The current histograms revealed a unitary conductance of 95–110 pS.

but we performed a more quantitative analysis. Even for cationic tracers (EB and PI and possibly NB), our data indicate that homotypic Cx26 channels are more permeant than homotypic Cx30 channels.

With scrape loading, we found that cells coexpressing Cx26 and Cx30 showed an intermediate degree of permeability to anionic dyes (LY, CF) than did cells expressing Cx26. These findings confirm the work of Sun et al. (49), who found that AlexaFluor 488 (an anionic dye) spreads between cells coexpressing Cx26-EGFP and Cx30-EGFP but not between cells expressing Cx30-EGFP alone but contradict a previous report that HeLa cells coexpressing Cx26 and Cx30 did not transfer injected anionic dyes Cascade blue or LY (39). Technical issues may account for their failure to find transfer of these dyes, including the fact that cells were injected and that rat

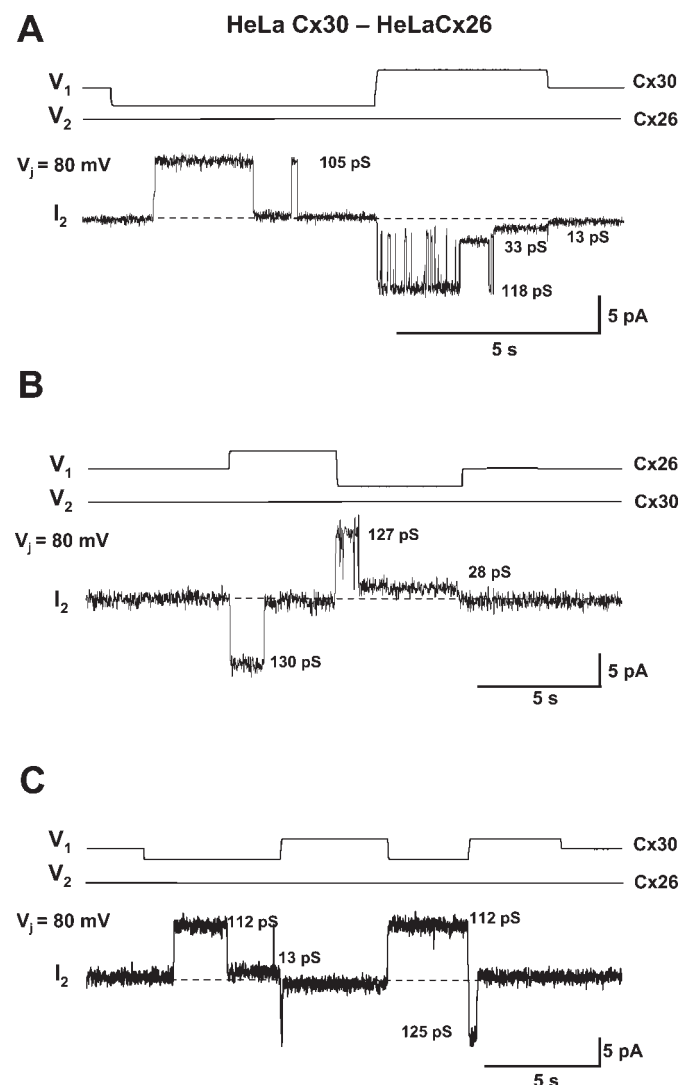


Fig. 9. Single-channel properties of heterotypic Cx26-Cx30 gap junctions. Current records with 1 operational channel from heterotypic Cx30-Cx26 cell pairs are shown. *A*: bipolar pulse protocol ($V_1 = \pm 80$ mV, voltage stepped in Cx30 cell and voltage held constant in Cx26 cell, $V_2 = 0$ mV) and related junctional current (I_2) recorded from Cx26 cell. Hyperpolarization of the Cx30 cell produced a main $\gamma_j = 105$ pS, whereas depolarization yielded several unitary conductance values: main $\gamma_j = 118$ pS, residual $\gamma_j = 13$ pS, and substate $\gamma_j = 33$ pS. *B*: depolarization of the Cx26 cell (voltage stepped in Cx26 cell and voltage held constant in Cx30) produced a single main $\gamma_j = 130$ pS, whereas hyperpolarization gave main $\gamma_j = 127$ pS and residual $\gamma_j = 28$ pS. *C*: subsequent hyperpolarization and depolarization of Cx30 cell yielded a main γ_j of 112 and 125 pS, respectively. The channel open time exhibited voltage dependency; i.e., channel remained longer in main state when Cx30 cell was negative.

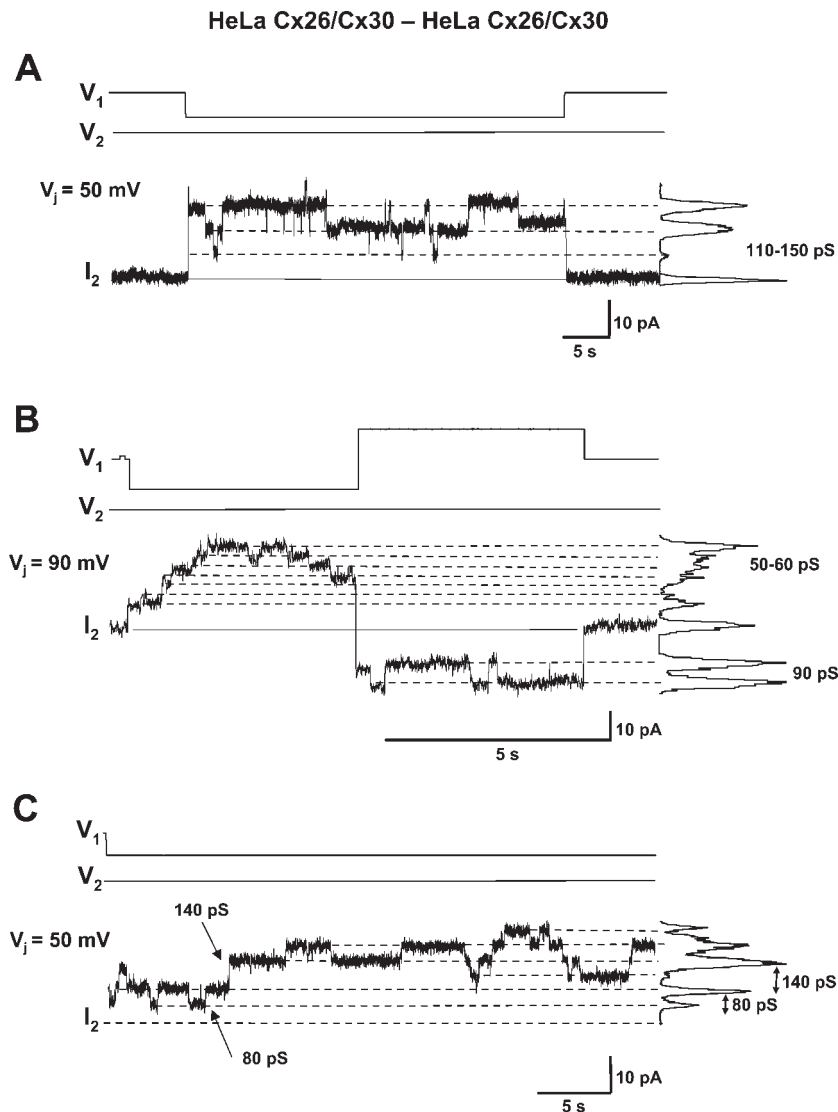


Fig. 10. Single-channel properties of cotransfected Cx26/Cx30 cells. Current records were obtained from HeLa cells cotransfected with Cx26 and Cx30. *A*: multichannel recording of cell pairs during a maintained V_j of 50 mV. Current histograms revealed unitary conductances of 110–150 pS. Solid line, zero current level; dashed lines, discrete current steps indicative of opening and closing of channels. *B*: multichannel recording during a bipolar V_j of ± 90 mV. Current histograms yielded different unitary conductances of 90 and 50–60 pS for negative and positive V_j , respectively, indicating the presence of nonhomotypic channels. *C*: multichannel recording during a maintained V_j of 50 mV. The current histograms suggest the operation of at least 2 different channels with conductances of 80 and 140 pS (arrows), which resemble homotypic Cx26 and homotypic Cx30 channels, respectively.

Cx26 and mouse Cx30 were used. In addition, our observation that NB and PI diffused further in cells that express both Cx26 and Cx30 than in cells that express either one alone is consistent with quantitative differences in the diffusion of Ca^{2+} reported by Sun et al. (49). Thus channels from cells that express both Cx26 and Cx30 appear to have an “emergent property” that is distinct from that of their individual components, but the nature of the heterotypic channel is not clear.

Furthermore, we extended the investigation of the permeability of these cells with FRAP (10, 61), demonstrating that both the rate and the amount of calcein transferred between cells coexpressing Cx26 and Cx30 were intermediate to those in cells expressing Cx26 or Cx30 alone. Without the sensitivity of FRAP, we would not have detected that Cx30 homotypic channels were slightly permeable to calcein. For analysis of monolayers of cells, FRAP is highly reproducible, thereby allowing an unprecedented, quantitative analysis of dye diffusion through gap junctions.

Cx26 and Cx30 form functional heterotypic channels. We used a novel adaptation of FRAP to show that the transfer of calcein (an anionic dye) through Cx26-Cx30 heterotypic chan-

nels was intermediate between homotypic channels composed of Cx26 (which transferred calcein robustly) and Cx30 (which transferred calcein minimally). Thus one connexin does not completely determine the permeability of a heterotypic pair; these differences were not noted in a prior study that used NB only (37). Prior studies (injecting one cell of a cell pair) indicate that other combinations of heterotypic channels [e.g., Cx40-Cx43 (55), Cx26-Cx32 (11)] have intermediate levels of dye transfer compared with their homotypic counterparts (15).

Voltage gating of Cx26 and Cx30 mixed channels. The voltage-gating properties of homotypic Cx26 and Cx30 channels that we and others have documented *in vitro* are not directly comparable to the data obtained from isolated pairs of cochlear supporting cells, which show asymmetrical voltage gating (53, 70). Thus simple homotypic Cx26 or Cx30 channels cannot explain the voltage gating seen in cochlear supporting cells, in which Cx26 and Cx30 have been proposed to form heteromeric and/or heterotypic gap junction channels with variable stoichiometry (70). The voltage-dependent behavior of the macroscopic junctional currents that we recorded here between both Cx26-Cx30 heterotypic and Cx26/Cx30

heteromeric cell pairs closely resembled the complex voltage dependence recorded in primary cochlear supporting cells, indicating that Cx26 and Cx30 form mixed channels in supporting cells. The single-channel properties of cells expressing both Cx26 and Cx30 are more complex. Despite altered junctional permeability and biochemical evidence that support heteromeric channel formation, we cannot clearly distinguish heteromeric channels from heterotypic ones based on the unitary conductance data alone.

Implications for disease. It has been proposed that mutations in *GJB2/Cx26*, *GJB6/Cx30*, *KCNQ1*, *KCNQ4*, and *KCNE1* cause hearing loss by disrupting K^+ recycling in the cochlea (32, 45, 47). The variable overlapping expression of Cx26 and Cx30 in the cochlear supporting cells may result in the asymmetrical voltage gating (70) that has been hypothesized to directionally funnel K^+ away from the sensory cells after acoustic stimulation (53, 69). If heteromeric and/or heterotypic channels are required for K^+ recycling, then the loss of either Cx26 or Cx30 would disrupt K^+ homeostasis because neither one can compensate for the loss of the other in this regard.

Other data suggest that the role of gap junctional communication in the cochlea may not be limited to K^+ recycling. For example, targeted ablation of Cx26 in the cochlear epithelium causes hearing impairment and progressive death of hair cells but does not alter the expression of Cx30 or affect the endocochlear potential before the onset of cell death (13). Similarly, the pattern of Cx26 expression in the cochlea is not affected in *Gjb6/Cx30*-null mice, which also develop hearing loss (50). Despite the above arguments, it is problematic that Cx26 and Cx30 do not compensate for each other in these animal models because both homotypic Cx26 and homotypic Cx30 channels are permeable to K^+ (37, 57), and Cx26 and Cx30 have broadly overlapping (but not identical) distributions and a similar profile of developmental expression (2, 23, 28, 49, 71). Finally, some Cx26 mutants that are associated with hearing loss have no abnormal electrophysiological characteristics, including K^+ permeability, but have impaired permeability to inositol 1,4,5-trisphosphate passage (6, 68).

The selectivity for size and charge, as well as the temporal and kinetic differences in the permeability to charged molecules, of homotypic Cx26-Cx26, homotypic Cx30-Cx30, and heterotypic (and likely heteromeric) Cx26-Cx30 channels demonstrated by this and other studies may be relevant to this issue. The discrepancies between the results found in cells that express both Cx26 and Cx30 as opposed to only one of these connexins form the basis for this inference. Thus cells expressing both Cx26 and Cx30 have faster intercellular Ca^{2+} signaling (49) and are more permeable to NB (this study). This has been better demonstrated for Cx26-Cx32 heteromeric channels, which are selectively permeable to cAMP, cGMP, and inositol 1,4,5-trisphosphate unlike the corresponding homotypic channels (36).

Given these considerations, it is quite surprising that overexpression of the mouse *Gjb2/Cx26* gene (as a transgene) can rescue hearing loss in *Gjb6/Cx30*-null mice (3). The *Gjb2/Cx26* transgene restores the level of Cx26 protein, which is reduced in *Gjb6/Cx30*-null mice, and prevents the degeneration of the cochlea. According to these findings, heteromeric Cx26-Cx30 channels do not appear to be required for normal hearing; the amount of Cx26 protein seems to be key. Given this result, it would be informative to replace the *Gjb6/Cx30* gene with the

Gjb2/Cx26 gene, as comparable gene replacements in the lens (62) and heart (42) did not completely “rescue” the phenotype of the missing connexin.

ACKNOWLEDGMENTS

We thank Dr. Bruce Nicholson for providing the human Cx26 cDNA, Dr. Klaus Willecke for the HeLa cells, Dr. Hajime Takano for advice, Dr. Edward Cooper for use of equipment, and Alan Enriquez for technical support.

GRANTS

This work was supported by National Institutes of Health Grants KO8 DC-005394 (to S. W. Yum), RO1 NS-42878 and NS-043560 (to S. S. Scherer), RO1 DC-006652 and RO1 EY-013163 (to T. W. White), and GM-055263 and EY-014604 (to P. R. Brink); American Heart Association Grant 0335236N (to V. Valiunas); and subcontract and National Institutes of Health Grant P30 NS-047321, which supports the Center for Dynamic Imaging of Nervous System Function, where the FRET and FRAP experiments were performed.

REFERENCES

1. Abraham V, Chou ML, George P, Pooler P, Zaman A, Savani RC, Koval M. Heterocellular gap junctional communication between alveolar epithelial cells. *Am J Physiol Lung Cell Mol Physiol* 280: L1085–L1093, 2001.
2. Ahmad S, Chen SP, Sun JJ, Lin X. Connexins 26 and 30 are co-assembled to form gap junctions in the cochlea of mice. *Biochem Biophys Res Commun* 307: 362–368, 2003.
3. Ahmad S, Tang W, Chang Q, Qu Y, Hibshman J, Li Y, Sohl G, Willecke K, Chen P, Lin X. Restoration of connexin26 protein level in the cochlea completely rescues hearing in a mouse model of human connexin30-linked deafness. *Proc Natl Acad Sci USA* 104: 1337–1341, 2007.
4. Barrio LC, Capel J, Jarillo JA, Castro C, Revilla A. Species-specific voltage-gating properties of connexin-45 junctions expressed in *Xenopus* oocytes. *Biophys J* 73: 757–769, 1997.
5. Beltramello M, Bicego M, Piazza V, Ciubotaru CD, Mammano F, DAndrea P. Permeability and gating properties of human connexins 26 and 30 expressed in HeLa cells. *Biochem Biophys Res Commun* 305: 1024–1033, 2003.
6. Beltramello M, Piazza V, Bukauskas FF, Pozzan T, Mammano F. Impaired permeability to $Ins(1,4,5)P_3$ in a mutant connexin underlies recessive hereditary deafness. *Nat Cell Biol* 7: 63–69, 2005.
7. Brink PR, Cronin K, Banach K, Peterson E, Westphale EM, Seul KH, Ramanan SV, Beyer EC. Evidence for heteromeric gap junction channels formed from rat connexin43 and human connexin37. *Am J Physiol Cell Physiol* 273: C1386–C1396, 1997.
8. Bruzzone R, White TW, Paul DL. Connections with connexins: the molecular basis of direct intercellular signaling. *Eur J Biochem* 238: 1–27, 1996.
9. Bukauskas FF, Bukauskiene A, Bennett MV, Verselis VK. Gating properties of gap junction channels assembled from connexin43 and connexin43 fused with green fluorescent protein. *Biophys J* 81: 137–152, 2001.
10. Cameron SJ, Malik S, Akaike M, Lerner-Marmarosh N, Yan C, Lee JD, Abe J, Yang J. Regulation of epidermal growth factor-induced connexin 43 gap junction communication by big mitogen-activated protein kinase1/ERK5 but not ERK1/2 kinase activation. *J Biol Chem* 278: 18682–18688, 2003.
11. Cao FL, Eckert R, Elfgang C, Nitsche JM, Snyder SA, Hulser DF, Willecke K, Nicholson BJ. A quantitative analysis of connexin-specific permeability differences of gap junctions expressed in HeLa transfectants and *Xenopus* oocytes. *J Cell Sci* 111: 31–43, 1998.
12. Clegg RM. Fluorescence resonance energy transfer. *Curr Opin Biotechnol* 6: 103–110, 1995.
13. Cohen-Salmon M, Ott T, Michel V, Hardelin JP, Perfettini I, Eybalin M, Wu T, Marcus DC, Wangemann P, Willecke K, Petit C. Targeted ablation of connexin26 in the inner ear epithelial gap junction network causes hearing impairment and cell death. *Curr Biol* 12: 1106–1111, 2002.
14. Common JEA, Becker D, Di WL, Leight IM, O’Toole EA, Kelsell DP. Functional studies of human skin disease- and deafness-associated connexin 30 mutations. *Biochem Biophys Res Commun* 298: 651–656, 2002.

15. Cottrell GT, Burt JM. Functional consequences of heterogeneous gap junction channel formation and its influence in health and disease. *Biochim Biophys Acta* 1711: 126–141, 2005.
16. Di WL, Gu Y, Common JEA, Aasen T, O'Toole EA, Kessel DP, Zicha D. Connexin interaction patterns in keratinocytes revealed morphologically and by FRET analysis. *J Cell Sci* 118: 1505–1514, 2005.
17. Eckert R. Gap-junctional single-channel permeability for fluorescent tracers in mammalian cell cultures. *Biophys J* 91: 565–579, 2006.
18. Eckert R, Dunina-Barkovskaya A, Hulser DF. Biophysical characterization of gap-junction channels in HeLa cells. *Pflügers Arch* 424: 335–342, 1993.
19. Eifgang C, Eckert R, Lichternberg-Frate H, Butterweck A, Traub O, Klein RA, Hulser DF, Willecke K. Specific permeability and selective formation of gap junction channels in connexin-transfected HeLa cells. *J Cell Biol* 129: 805–817, 1995.
20. El-Fouly M, Trosko J, Chang C. Scrape-loading and dye transfer. A rapid and simple technique to study gap junctional intercellular communication. *Exp Cell Res* 168: 422–430, 1987.
21. Fawcett DW. *The Cell*. Philadelphia, PA: Saunders, 1981.
22. Forge A, Becker D, Casalotti S, Edwards J, Marziano N, Nevill G. Gap junctions in the inner ear: comparison of distribution patterns in different vertebrates and assessment of connexin composition in mammals. *J Comp Neurol* 467: 207–229, 2003.
23. Forge A, Becker D, Casalotti S, Edwards J, Marziano N, Nickel R. Connexins and gap junctions in the inner ear. *Audiol Neurootol* 7: 141–145, 2002.
24. Gemel J, Valiunas V, Brink PR, Beyer EC. Connexin43 and connexin26 form gap junctions, but not heteromeric channels in co-expressing cells. *J Cell Sci* 117: 2469–2480, 2004.
25. Gonzalez D, Gomez-Hernandez JM, Barrio LC. Species specificity of mammalian connexin-26 to form open voltage-gated hemichannels. *FASEB J* 20: 2329–2338, 2006.
26. Gu Y, Di W, Kessel D, Zicha D. Quantitative fluorescence resonance energy transfer (FRET) measurement with acceptor photobleaching and spectral unmixing. *J Microsc* 215: 162–173, 2004.
27. Hulser DF, Rehkopf B, Traub O. Dispersed and aggregated gap junction channels identified by immunogold labeling of freeze-fractured membranes. *Exp Cell Res* 233: 240–251, 1997.
28. Jagger DJ, Forge A. Compartmentalized and signal-selective gap junctional coupling in the hearing cochlea. *J Neurosci* 26: 1260–1268, 2006.
29. Kenworthy A. Peering inside lipid rafts and caveolae. *Trends Biochem Sci* 27: 435–437, 2002.
30. Kenworthy AK, Edidin M. Distribution of a glycosylphosphatidylinositol-anchored protein at the apical surface of MDCK cells examined at a resolution of <100 Å using imaging fluorescence resonance energy transfer. *J Cell Biol* 142: 69–84, 1998.
31. Kenworthy AK, Petranova N, Edidin M. High-resolution FRET microscopy of cholera toxin B-subunit and GPI-anchored proteins in cell plasma membranes. *Mol Biol Cell* 11: 1645–1655, 2000.
32. Kikuchi T, Adams JC, Miyabe Y, So E, Kobayashi T. Potassium ion recycling pathway via gap junction systems in the mammalian cochlea and its interruption in hereditary nonsyndromic deafness. *Med Electron Microsc* 33: 51–56, 2000.
33. Kikuchi T, Kimura RS, Paul DL, Adams JC. Gap junctions in the rat cochlea: immunohistochemical and ultrastructural analysis. *Anat Embryol (Berl)* 191: 101–118, 1995.
34. Kumar NM, Gilula NB. The gap junction communication channel. *Cell* 84: 381–389, 1996.
35. Lautermann J, tenCate WJF, Altenhoff P, Grummer R, Traub O, Frank HG, Jahnke K, Winterhager E. Expression of the gap-junction connexins 26 and 30 in the rat cochlea. *Cell Tissue Res* 294: 415–420, 1998.
36. Locke D, Stein T, Davies C, Morris J, Harris AL, Evans WH, Monaghan P, Gusterson B. Altered permeability and modulatory character of connexin channels during mammary gland development. *Exp Cell Res* 298: 643–660, 2004.
37. Manthey D, Banach K, Desplantez T, Lee CG, Kozak CA, Traub O, Weingart R, Willecke K. Intracellular domains of mouse connexin26 and-30 affect diffusional and electrical properties of gap junction channels. *J Membr Biol* 181: 137–148, 2001.
38. Martin PEM, Coleman SL, Casalotti SO, Forge A, Evans WH. Properties of connexin26 gap junctional proteins derived from mutations associated with nonsyndromal hereditary deafness. *Hum Mol Genet* 8: 2369–2376, 1999.
39. Marziano NK, Casalotti SO, Portelli AE, Becker DL, Forge A. Mutations in the gene for connexin 26 (GJB2) that cause hearing loss have a dominant negative effect on connexin 30. *Hum Mol Genet* 12: 805–812, 2003.
40. Nagy JI, Ochalski PAY, Li J, Hertzberg EL. Evidence for the colocalization of another connexin with connexin-43 at astrocytic gap junctions in rat brain. *Neuroscience* 78: 533–548, 1997.
41. Ormo M, Cubitt AB, Kallio K, Gross LA, Tsien RY, Remington SJ. Crystal structure of the *Aequorea victoria* green fluorescent protein. *Science* 273: 1392–1395, 1996.
42. Plum A, Hallas G, Magin T, Dombrowski F, Hagendorff A, Schumacher B, Wolpert C, Kim JS, Lamers WH, Evert M, Meda P, Traub O, Willecke K. Unique and shared functions of different connexins in mice. *Curr Biol* 10: 1083–1091, 2000.
43. Rabionet R, Gasparini P, Estivill X. Molecular genetics of hearing impairment due to mutations in gap junction genes encoding beta connexins. *Hum Mutat* 16: 190–202, 2000.
44. Richard G. Connexin gene pathology. *Clin Exp Dermatol* 28: 397–409, 2003.
45. Santos-Sacchi J. The effects of cytoplasmic acidification upon electrical coupling in the organ of Corti. *Hear Res* 19: 207–215, 1985.
46. Silvius JR. Fluorescence energy transfer reveals microdomain formation at physiological temperatures in lipid mixtures modeling the outer leaflet of the plasma membrane. *Biophys J* 85: 1034–1045, 2003.
47. Steel KP. Perspectives, biomedicine: the benefits of recycling. *Science* 285: 1363–1364, 1999.
48. Sullivan R, Lo CW. Expression of a connexin 43/beta-galactosidase fusion protein inhibits gap junctional communication in NIH3T3 cells. *J Cell Biol* 130: 419–429, 1995.
49. Sun JJ, Ahmad S, Chen SP, Tang WX, Zhang YP, Chen P, Lin X. Cochlear gap junctions coassembled from Cx26 and 30 show faster intercellular Ca²⁺ signaling than homomeric counterparts. *Am J Physiol Cell Physiol* 288: C613–C623, 2005.
50. Teubner B, Michel V, Pesch J, Lautermann J, Cohen Salmon M, Sohl G, Jahnke K, Winterhager E, Herberhold C, Hardelin JP, Petit C, Willecke K. Connexin30 (Gjb6)-deficiency causes severe hearing impairment and lack of endocochlear potential. *Hum Mol Genet* 12: 13–21, 2003.
51. Thomas T, Aasen T, Hodgins M, Laird DW. Transport and function of cx26 mutants involved in skin and deafness disorders. *Cell Commun Adhes* 10: 353–358, 2003.
52. Thomas T, Jordan K, Simek J, Shao Q, Jedeszko C, Walton P, Laird DW. Mechanisms of Cx43 and Cx26 transport to the plasma membrane and gap junction regeneration. *J Cell Sci* 118: 4451–4462, 2005.
53. Todt I, Ngezahayo A, Ernst A, Kolb HA. Hydrogen peroxide inhibits gap junctional coupling and modulates intracellular free calcium in cochlear Hensen cells. *J Membr Biol* 181: 107–114, 2001.
54. Unger VM, Kumar NM, Gilula NB, Yeager M. Projection structure of a gap junction membrane channels at 7 Å resolution. *Nat Struct Biol* 4: 1997.
55. Valiunas V, Beyer EC, Brink PR. Cardiac gap junction channels show quantitative differences in selectivity. *Circ Res* 91: 104–111, 2002.
56. Valiunas V, Gemel J, Brink PR, Beyer EC. Gap junction channels formed by coexpressed connexin40 and connexin43. *Am J Physiol Heart Circ Physiol* 281: H1675–H1689, 2001.
57. Valiunas V, Manthey D, Vogel R, Willecke K, Weingart R. Biophysical properties of mouse connexin30 gap junction channels studied in transfected human HeLa cells. *J Physiol* 519: 631–644, 1999.
58. Valiunas V, Niessen H, Willecke K, Weingart R. Electrophysiological properties of gap junction channels in hepatocytes isolated from connexin32-deficient and wild-type mice. *Pflügers Arch* 437: 846–856, 1999.
59. Valiunas V, Polosina YY, Miller H, Potapova IA, Valiuniene L, Doronin S, Mathias RT, Robinson RB, Rosen MR, Cohen IS, Brink PR. Connexin-specific cell-to-cell transfer of short interfering RNA by gap junctions. *J Physiol* 568: 459–468, 2005.
60. Valiunas V, Weingart R, Brink PR. Formation of heterotypic gap junction channels by connexins 40 and 43. *Circ Res* 86: E42–E49, 2000.

61. **Wade MH, Trosko JE, Schindler M.** A fluorescence photobleaching assay of gap junction-mediated communication between human cells. *Science* 232: 525–528, 1986.
62. **White TW.** Nonredundant gap junction functions. *News Physiol Sci* 18: 95–99, 2003.
63. **White TW, Bruzzone R.** Multiple connexin proteins in single intercellular channels: connexin compatibility and functional consequences. *J Bioenerg Biomembr* 28: 339–350, 1996.
64. **Willecke K, Eiberger J, Degen J, Eckardt D, Romualdi A, Guldenagel M, Deutsch U, Söhl G.** Structural and functional diversity of connexin genes in the mouse and human genome. *Biol Chem* 383: 725–737, 2002.
65. **Wu P, Brand L.** Resonance energy transfer: methods and applications. *Anal Biochem* 218: 1–13, 1994.
66. **Yum SW, Kleopa KA, Shumas S, Scherer SS.** Diverse trafficking abnormalities for connexin32 mutants causing CMTX. *Neurobiol Dis* 11: 43–52, 2002.
67. **Zacharias DA, Violin JD, Newton AC, Tsien RY.** Partitioning of lipid-modified monomeric GFPs into membrane microdomains of live cells. *Science* 296: 913–916, 2002.
68. **Zhang Y, Tang W, Ahmad S, Sipp JA, Chen P, Lin X.** Gap junction-mediated intercellular biochemical coupling in cochlear supporting cells is required for normal cochlear functions. *Proc Natl Acad Sci USA* 102: 15201–15206, 2005.
69. **Zhao HB, Kikuchi T, Ngezahayo A, White TW.** Gap junctions and cochlear homeostasis. *J Membr Biol* 209: 177–186, 2006.
70. **Zhao HB, Santos-Sacchi J.** Voltage gating of gap junctions in cochlear supporting cells: evidence for nonhomotypic channels. *J Membr Biol* 175: 17–24, 2000.
71. **Zhao HB, Yu N.** Distinct and gradient distributions of Connexin26 and Connexin30 in the cochlear sensory epithelium of guinea pigs. *J Comp Neurol* 499: 506–518, 2006.

